

RESEARCH ARTICLE

10.1029/2017TC004843

Special Section:

An appraisal of Global Continental Crust: Structure and Evolution

Key Points:

- Moho depths and Vp/Vs ratios increase near major Proterozoic boundary zones
- The MHB-Wyoming suture resides within the Trans-Montana Orogen, distinct from potential field gradients
- High Vp/Vs ratio and lower crustal P-to-S conversions suggest underplating along the GFTZ

Supporting Information:

- Supporting Information S1

Correspondence to:

Y. Chen,
yunfeng1@ualberta.ca

Citation:

Gu, Y. J., Chen, Y., Dokht, R. M. H., & Wang, R. (2018). Precambrian tectonic discontinuities in western Laurentia: Broadband seismological perspectives on the Snowbird and Great Falls tectonic zones. *Tectonics*, 37. <https://doi.org/10.1029/2017TC004843>

Received 10 OCT 2017

Accepted 8 APR 2018

Accepted article online 20 APR 2018

Precambrian Tectonic Discontinuities in Western Laurentia: Broadband Seismological Perspectives on the Snowbird and Great Falls Tectonic Zones

Yu Jeffrey Gu¹, Yunfeng Chen¹ , Ramin M. H. Dokht² , and Ruijia Wang¹ 

¹Department of Physics, University of Alberta, Edmonton, Alberta, Canada, ²Geological Survey of Canada, Sidney, British Columbia, Canada

Abstract The Snowbird Tectonic Zone (STZ) in southwestern Canada and the Great Falls Tectonic Zone (GFTZ) in northern Montana are two structural lineaments with major implications for the formation and evolution of the western North American craton. In this study, we examine the origins of these two proposed Proterozoic sutures using broadband seismic data from Alberta and USAArray stations. We find substantial spatial variations in crustal structure and thickness across both the STZ and GFTZ based on an integrated analysis of *P*-to-*S* receiver functions, shear velocities, and potential field measurements. The STZ marks the transition from deep (NW, ~44 km) to shallow (SE, ~39 km) Moho in central Alberta. This steep Moho relief, in conjunction with elevated Vp/Vs ratios, provide compelling evidence for Proterozoic subduction and magmatism. In northern Montana, the Moho is depressed by ~6 km within the fold-and-thrust belts of the Trans-Montana Orogen, where high (>1.84) Vp/Vs ratios spread along the collisional suture of the Dillion Shear Zone and terminates sharply along the reworked margin of the Wyoming craton. These observations, coupled with widespread lower crustal conversions, are concordant with a Paleoproterozoic orogeny resulting from collision(s) between Archean cratons. On the other hand, a flat Moho under major northeast striking potential field lineaments in the northernmost Montana favors an origin as a ductile shear zone, rather than suture, in the orogenic hinterland. We find evidence for crustal underplating beneath the GFTZ, though this anomalous layer is smaller than previous estimates and appears to be confined to the Trans-Montana Orogen.

1. Introduction

The lithosphere beneath the Western Canada Sedimentary Basin (WCSB) and northern Montana contains vital records of the Precambrian tectonic development of western Laurentia (Hoffman, 1988; Ross et al., 1991). While much of the basement is inaccessible to direct geological sampling due to extensive Phanerozoic sedimentation (e.g., Ross et al., 1991; Villeneuve et al., 1993), especially in southern Alberta and northern Montana near the Rocky mountain foredeep, geological (Hoffman, 1988, 1989; O'Neill & Lopez, 1985; Pana, 2003; Sims et al., 2004; Sims et al., 2005), potential field (Boerner et al., 2000; Nieuwenhuis et al., 2014), geochemical (Aulbach et al., 2004; Buhlmann et al., 2000; Burwash et al., 2000; Chacko et al., 2000; Davis et al., 1995; Mueller & Frost, 2006; Ross et al., 1991; Villeneuve et al., 1993), and seismological (Bouzidi et al., 2002; Chen et al., 2017; Chen et al., 2015; Clowes et al., 2002; Eaton & Cassidy, 1996; Gu et al., 2011, 2015; Gu & Shen, 2015; Ross et al., 2000; Schulte-Pelkum et al., 2017) observations have provided compelling evidence for an intricate regional tectonic framework consisting of more than 20 Precambrian domains (Ross et al., 1991) and ancient bedrocks dating as far back as ~3.4 Ga (Mueller & Frost, 2006; Sims et al., 2004). Precambrian events in this region are highlighted by three proposed tectonic discontinuities, the east-northeast trending Snowbird Tectonic Zone (STZ) across central Alberta, Vulcan Structure (VS) in southern Alberta, and Great Falls Tectonic Zone (GFTZ) in northern Montana (Figure 1a). All three structures have been linked to quasi-linear trends in potential field data (e.g., Gorman et al., 2002; Hope & Eaton, 2002; O'Neill & Lopez, 1985; Ross et al., 1991) and are most commonly viewed as Precambrian collision boundaries associated with, from north to south, the Archean Hearne province, Medicine Hat Block (MHB) and Wyoming craton (Hoffman, 1988, 1989; O'Neill & Lopez, 1985; Ross et al., 1991).

Identification and interpretations of the STZ and GFTZ are fundamental to the understanding of craton formation and evolution in western Laurentia. Unfortunately, largely due to limited surface geological exposure and two-dimensional (2-D) receiver geometries, the task of validating the crustal imprints and origins of

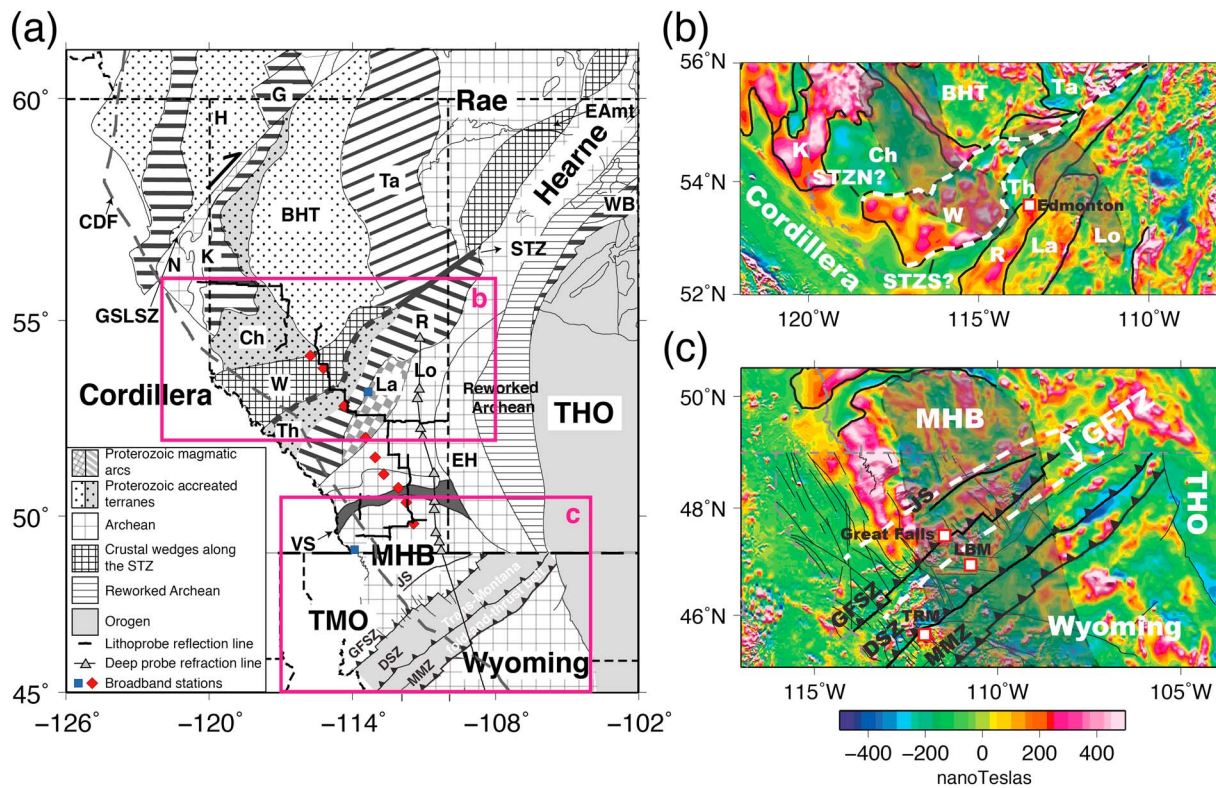


Figure 1. (a) Tectonic map of western Laurentia, modified after Ross et al. (1991). The two proposed tectonic boundaries (Snowbird Tectonic Zone, STZ and Great Falls Tectonic Zone, GFTZ) are highlighted by the red rectangles. (b) Aeromagnetic field strengths within the highlighted region (see Figure 1a) around the STZ. The white dashed lines mark the earlier-proposed (e.g., Ross & Eaton, 2002; Ross et al., 1991) northern (STZN) and southern (STZS) branches of the STZ. The shaded areas show the distributions of mafic (west) and felsic (east) magmatic intrusions imaged by earlier geophysical analyses (Bouzidi et al., 2002; Chen et al., 2015; Ross, 2002; Ross & Eaton, 1997; Welford & Clowes, 2006). (c) Aeromagnetic anomalies within the highlighted region (see Figure 1a) containing the GFTZ. The white dashed lines indicate the suggested location of the GFTZ based on NE trending aeromagnetic gradients (e.g., Gorman et al., 2002; Lemieux et al., 2000). The heavy harbed lines mark the fold-and-thrust belts of the Trans-Montana Orogen (TMO). The distribution of a high-velocity lower crustal layer (LCL) from Ross (2002) is indicated by the shaded region. “Great Falls” denotes the township location of Great Falls in northwestern Montana. Tobacco Root Mountain (TRM) and Little Belt Mountain (LBM) are two of the few locations showing the outcrop of the Precambrian basement rocks within the TMO. Abbreviations: BHT = Buffalo Head Terrane; Ch = Chinchaga; CDF = Cordilleran Deformation Front; DSZ = Dillon Shear Zone; EAm = East Athabasca mylonite triangle; EH = Eyehill High; G = Great Bear; GFSZ = Great Falls Shear Zone; GSLSZ = Great Slave Lake Shear Zone; H = Hottah; K = Ksituan; La = Lacombe; Lo = Loverna block; MMZ = Madison Mylonite Zone; MHB = Medicine Hat Block; N = Nova; R = Rimbey; STZ = Snowbird Tectonic Zone; STZN = northern STZ; STZS = southern STZ; Ta = Talton Magmatic Zone; Th = Thorsby; THO = Trans-Hudson Orogen; VS = Vulcan Structure; W = Wabamun.

these proposed structural boundaries has been challenging. For example, despite prominent potential field observations (e.g., Ross et al., 1991), which are the basis of domain definitions (Ross et al., 1991, 1993), seismic constraints on the location, depth, and nature of the STZ mostly relied on linear active-source experiments deployed sporadically across the study region. It remains speculative whether the STZ faithfully follows Rimbey (STZS in Figure 1b), a proposed magmatic arc (Chen et al., 2017; Eaton & Cassidy, 1996; Gibb & Walcott, 1971; Ross & Eaton, 2002) or bifurcates around the Proterozoic accreted Wabamun domain (Ross et al., 1991; STZN in Figure 1b). Instead of a collisional origin (Berman et al., 2007; Gibb & Walcott, 1971; Hoffman, 1988), alternative interpretations of the STZ as a Precambrian intracontinental shear zone (Boerner et al., 2000; Hanmer et al., 1994), rift (e.g., Flowers et al., 2006), or a reactivated block boundary (Regan et al., 2017) cannot be dismissed based on the existing data alone.

Similar to the STZ, seismic observations from active source experiments (Clowes et al., 2002; Gorman et al., 2002; Snellson et al., 1998) in southern Alberta and northern Montana offer only a limited window into the basement structure due to a thick sedimentary cover (Mueller & Frost, 2006; Sims et al., 2004). Among the key findings, P wave reflections recorded by the DEEP PROBE (Gorman et al., 2002) suggested the existence of a high-velocity lower crustal layer (LCL) beneath the MHB in southern Alberta, which deepens across the GFTZ along a southeast striking transect roughly parallel to the foothills of the Rocky Mountains (Figure 1c). This anomalous layer was interpreted as evidence for underplating (Clowes et al., 2002;

Gorman et al., 2002; Ross, 2000), a process commonly associated with the emplacement of ultramafic magma at the base of continental crust (Furlong & Fountain, 1986; Fyfe, 1992; Cox, 1993; see Thybo & Artemieva, 2013 for a review), during Archean (Clowes et al., 2002; Gorman et al., 2002) or Proterozoic (Mueller & Frost, 2006; O'Neill, 1998; Sims et al., 2004, 2005) collisions between the MHB and the Wyoming craton. While this model was partially supported by the outcomes of an active-source experiment in northwestern United States (i.e., CD-ROM; Karlstrom et al., 2005), the precise location (Gorman et al., 2002), age, and nature of the underplated layer remain debated. Furthermore, the east-west dimension of the LCL and its connection to the GFTZ is speculative since the existing interpretations (e.g., Clowes et al., 2002; Gorman et al., 2002; Ross, 2002) were exclusively based upon crustal structural variations along NS oriented 2-D seismic profiles (see Figure 1a).

Following the overwhelming success of the LITHOPROBE (Clowes et al., 2010; Ross, 2000) project, regional broadband seismic arrays such as USArray, Canadian Rockies and Alberta Network (CRANE, since 2006; Gu et al., 2011), Regional Alberta Observatory for Earthquake Studies Network (RAVEN, since 2012; Schultz & Stern, 2015), and TransAlta Dam Monitoring Network (TD; since 2012) opened a new chapter in the investigation of crustal and mantle seismic structures near the western boundary of the North American craton. A series of recent studies (e.g., Bao & Eaton, 2015; Bao et al., 2016; Chen et al., 2015, 2017; Gilbert, 2012; Gu et al., 2015; Gu & Shen, 2015; Kao et al., 2013; Schulte-Pelkum et al., 2017) are testaments to renewed scientific interests in verifying, validating, and improving the existing theories of regional tectonics beneath western Laurentia. In the spirit of the aforementioned efforts, the overarching goal of this study is to place the latest broadband seismic observations, as well as existing geological and geophysical constraints, within a self-consistent regional tectonic framework of western Laurentia. We aim to answer the following two fundamental questions:

1. What, and how significant, are the crustal and mantle seismic expressions of the STZ?
2. Where is the GFTZ based on broadband seismological crustal constraints and if/how is it linked to underplating?

By acquiring clues to these questions through updated broadband seismic observations, we are able to provide an unbiased appraisal of the existing hypotheses pertaining to the proposed boundary zones near the western margin of the North American craton. Our findings clearly favor the STZ and GFTZ as critical suture zones during the Paleoproterozoic amalgamation of microcontinents in western Laurentia.

2. Tectonic Setting

The region containing the WCSB and northern Montana represents an integral part of the western margin of Laurentia, also known as the North American craton, formed in the early Proterozoic eon (Hoffman, 1988, 1989). It was suggested that during the assembly process, a number of Archean crustal elements (e.g., Hearne, MHB, and Wyoming) collided and were sutured together at orogenic belts and magmatic arcs (Hoffman, 1988; Ross et al., 1991). The following sections will formally introduce the STZ and GFTZ, two possible collisional boundaries within this tectonic framework.

2.1. Snowbird Tectonic Zone

The northeast trending STZ is one of the most recognizable geological structures across the North American craton. Originally proposed as an inter-continental suture (Gibb & Walcott, 1971; Hoffman, 1988; Ross et al., 1995, 2000), the nature of the 2,800+ km-long STZ remains a source of contentious debate. Along exposed segments of the STZ west of the Hudson Bay, discoveries of exhumation-related mylonite based on metamorphic and U-Pb zircon data (Hanmer et al., 1995; Mahan & Williams, 2005) and ultrapotassium rocks (Cousens et al., 2001; Hanmer & Relf, 2000) are generally concordant with an Archean tectonic framework. This hypothesis is corroborated by crustal signatures in central STZ (e.g., Legs Lake shear zone), where ultrapotassium rocks exhibit common neo-Archean signatures from both sides and favor an intra-continental origin (Hanmer et al., 1995). However, medium- to high-pressure metamorphic rocks, microdiamonds, local crustal thickening in eastern STZ (1.9 Ga) (Berman et al., 2013; MacRae et al., 1996) and magmatic mafic dikes in central STZ (Heaman, 1994; Heaman & LeCheminant, 1993) are more indicative of Proterozoic subduction (Berman et al., 2007) and/or asthenospheric upwelling-induced incipient rifting (Flowers et al., 2006, 2008).

Our study mainly focuses on the Alberta segment of the STZ, located in the southwestern part of the east-vergent East Athabasca mylonite triangle (EAmT; Hanmer et al., 1995; Figure 1a). Despite the lack of surface

geology, this segment has been widely associated with Paleoproterozoic subduction of the Thorsby domain and the ensuing collision between the Wabamun domain and Hearne province (Berman et al., 2007; Hoffman, 1988, 1989; Ross et al., 1991, 2000; Ross & Eaton, 2002). These collisions are supported both by the discovery of 2.40 Ga old gabbro beneath the Thorsby domain, which was the proposed ocean basin, and by the presence of 1.78–1.85 Ga granitic rocks beneath the neighboring (southeast of the Thorsby) Rimbey domain, the associated magmatic arc (Ross et al., 1991). This interpretation was largely motivated by aerial magnetic data that exhibit subparallel zones with both negative (Thorsby) and positive (Rimbey) magnetic signatures (Ross et al., 1991, 1993; Figure 1b). While the direction of slab dip remains debated (e.g., Ross & Eaton, 2002; Whitmeyer & Karlstrom, 2007), an interplate origin is favored by an abrupt change of potential field signatures from the Talton Magmatic Zone, a key element of the Thelon orogeny (Chacko et al., 2000), to southern central Alberta across the STZ (see Figure 1b). Electromagnetic data (Boerner et al., 1995) rendered no recognizable signatures, but elevated levels of electrical conductivity south of the STZ, which was subsequently referred to as the “Red Deer High”, show evidence of graphitic metasedimentary rocks and iron formation within a Proterozoic foredeep sequence (Boerner et al., 1995; Nieuwenhuis et al., 2014). Most of the regional seismological investigations since the early 1990s have been supportive of a collisional tectonic framework. Pronounced upper crustal reflectors known as the “Winagami reflection sequence” were discovered through reflection surveys to the northwest of the STZ (Figure 1b), which may have originated from mafic intrusive sills formed during the syncollisional magmatic events (Ross & Eaton, 1997; Welford & Clowes, 2006). Directly southeast of the STZ, the crust potentially underwent anatetic melting due to plate convergence in the Proterozoic eon. According to an earlier proposed “Tectonic Vise” model (Ross et al., 2000), the Wabamun domain and Trans-Hudson Orogen (THO) both collided with Hearne province, resulting to a collisional Plateau (i.e., the Hearne province) entrapped by dual subduction zones during the Paleoproterozoic. Basal melting induced by crustal shortening provides a viable explanation for widespread midcrustal low-velocity zones (see Figure 1b; Chen et al., 2015) and granite intrusion in the upper crust beneath central Alberta (Bouzidi et al., 2002). It has been suggested that a thin crust belies this region due to early Proterozoic crustal delamination (Eaton et al., 1999; Lemieux et al., 2000), a hypothesis that will be examined by the observations of this study.

2.2. Great Falls Tectonic Zone

The origin of the GFTZ, a proposed suture zone extending from Idaho batholith to southwesternmost Saskatchewan (O'Neill & Lopez, 1985; Figure 1c), is no less controversial than that of the STZ. Easily recognizable from northeast trending topographic lineaments along mapped high-angle faults and shear zones (O'Neill & Lopez, 1985), this geological structure is truncated in the east by the Proterozoic THO (see Figure 1c), which suggests a precollisional origin (Boerner et al., 1998). Central GFTZ features exposed basement rocks in the Little Belt Mountains (LBM), where Precambrian (1.86 Ga) calc-alkaline metaigneous assemblages exhibit isotopic signatures characteristic of a convergent environment (Mueller et al., 2002) and is thereby referred to as the “Little Belt arc” (Foster et al., 2006; Whitmeyer & Karlstrom, 2007). In southwestern GFTZ (e.g., TRM, see Figure 1c), Archean gneisses may have experienced a ~1.77 Ga granulite facies metamorphic and partial melting event (Sims et al., 2005). The westernmost GFTZ terminates between the Archean provinces in southwest Montana and Paleoproterozoic crust in Idaho, though the exact boundary is obscured by later sedimentation and magmatic events (Foster et al., 2006). Immediately north of the GFTZ resides the southern MHB, which was at times incorporated into the southern Hearne (Holm & Schneider, 2002) or Wyoming (Cavell et al., 1993; Henstock et al., 1998) cratons, but is more likely to be an independent Archean microcontinent with divergent properties between its eastern and western halves (Eaton et al., 1999; Lemieux et al., 2000; Ross et al., 1991; Sims et al., 2005). The region south of the GFTZ is occupied by the Wyoming craton that contains Archean aged rocks dating back to 3.5 Ga (Mueller & Frost, 2006). It has been suggested that the Wyoming craton underwent significant modifications by the Laramide (80–55 Ma) deformation (Foster et al., 2006) and impingement of the Yellowstone hotspot (e.g., Dave & Li, 2016; Schutt et al., 2008).

Based largely on the geological mapping of the Salmon-Anaconda tectonic zone in northern Montana, O'Neill and Lopez (1985) extrapolated their observations with extensive fault/dike-swarm systems toward the northeast and proposed a 150–200-km wide, 1500+ km-long GFTZ (see Figure 1c). This broad zone is cross-cut by a series of northwest trending basement faults (O'Neill, 2007; Sims et al., 2004), extending into the interior of the Wyoming craton (Figure 1c). Mesoproterozoic tectonothermal overprinting and

basement control have been widely suggested in the region spanning northeastern Idaho batholiths and the cratonic basement of Montana (O'Neill, 1998; Sims et al., 2004). On the other hand, northeast trending fabrics in both gravity and magnetic field data in western Montana appear to be more concordant with earlier proposed plate edge structural discontinuities developed during Paleoproterozoic era (Ross et al., 1991; Sims et al., 2004; Thomas et al., 1987).

The GFTZ has been widely associated with Precambrian plate convergence (Clowes et al., 2002; Gorman et al., 2002; Hoffman, 1988; Mueller et al., 2002; O'Neill & Lopez, 1985; Porritt et al., 2014). However, some geochemical data in the presumed Canadian segment of the GFTZ share common signatures between the MHB and Wyoming craton, which favor the GFTZ as an intra-continental fault system/shear zone (Buhlmann et al., 2000) instead of a Proterozoic suture (Mueller et al., 2002). The GFTZ bears distinctive signatures from the Proterozoic (1.60–1.85 Ga; Hayden & Wehrenberg, 1960; Giletti, 1966), but minettes from the igneous complex in Milk River (Alberta) and Sweet Grass Hills (Montana) north of the GFTZ contain coarse-grained mantle xenoliths rich in phlogopite, mica, feldspar, clinopyroxene, and apatite (Buhlmann et al., 2000), consistent in age with those found in the interior of Wyoming craton (>2.5 Ga; Giletti, 1966). This intraplate hypothesis was supported by the lack of distinctive electromagnetic or magmatic arc signatures across the GFTZ to the south and the THO to the east (Boerner et al., 1998). For this reason, Boerner et al. (1998) questioned the role of the GFTZ as a suture zone during the Proterozoic assembly of western Laurentia. On the other hand, evidence of arc magmatism and thrust belt signatures south of the originally proposed GFTZ (Sims et al., 2004) clearly favors plate convergence and subduction (Mueller et al., 2002; Mueller & Frost, 2006; O'Neill & Lopez, 1985).

Since the original discovery of the GFTZ by O'Neill and Lopez (1985), the understanding of this highly deformed region has been greatly advanced through multidisciplinary investigations, though its interpretations suffered from inconsistent, often confusing, definitions from geophysical, geological, and geochemical perspectives. One of such complications is the location of the GFTZ with respect to major structural lineaments in northwestern Montana, which, from north to south, are Joplin Structure (JS), Great Falls Shear Zone (GFSZ), Dillon Shear Zone (DSZ), and Madison Mylonite Zone (MMZ; see Figure 1c). Among these faults, the JS coincides with a linear trend of potential field (magnetic and gravity) anomalies, which outlines the northern boundary of the GFTZ in earlier geophysical investigations (e.g., Boerner et al., 1998; Clowes et al., 2002; Gorman et al., 2002; Lemieux et al., 2000). The southern boundary of the GFTZ was then defined either as the linear negative gravity gradient near the JS (e.g., Clowes et al., 2002; Gorman et al., 2002) or the southern edge of northeast trending magnetic fabrics slightly north of the GFSZ (e.g., Boerner et al., 1998; Lemieux et al., 2000). By this definition, the GFTZ is a relatively narrow geological boundary zone confined within these two potential field lineaments. Alternatively, the GFSZ was defined as the northern limit of the GFTZ in recent geological and geochemical analyses (e.g., Buhlmann et al., 2000; Mueller et al., 2002; Mueller & Frost, 2006; Foster et al., 2006). According to this hypothesis, the GFTZ extends southeastward to the DSZ, possibly reaching as far as the MMZ (Sims et al., 2004, 2005). The apparent discrepancies in the location and dimension of the GFTZ are largely responsible for its questionable role during the assembly of western Laurentia.

Regardless of the nature of the GFTZ, the crusts of both the MHB and Wyoming craton exhibit isotopic signatures consistent with an overprinted lower crust due to a mantle enrichment event during the Paleoproterozoic era (Buhlmann et al., 2000; Levander & Miller, 2012). With a *P* wave velocity exceeding 7 km/s, this mafic LCL (Gorman et al., 2002; Clowes et al., 2002; Levander & Miller, 2012; see Figure 1c) has been linked to concurrent Proterozoic collisions along the THO in the east and an orogenic belt near the western margin of MHB-Wyoming system (Davis et al., 1995; Mueller et al., 1995). The top and bottom of the LCL have been mainly delineated through active source seismic data (see Figure 1), which jointly suggest a thickened crust beneath the southeastern MHB and the northern Wyoming craton across and/or along the GFTZ (Clowes et al., 2002; Gorman et al., 2002; Ross, 2002).

3. Data and Method

The main goal of this study is to assess the robustness of key observations of the STZ and GFTZ, two proposed structural discontinuities vital for the understanding of the tectonic evolution of western Laurentia. To accomplish this, we combine new crustal seismic observations based on the most complete broadband station coverage in the WCSB and northern Montana, coupled with existing constraints from recently published studies of this region. Our latest regional data consist of recordings from three stations from Canadian

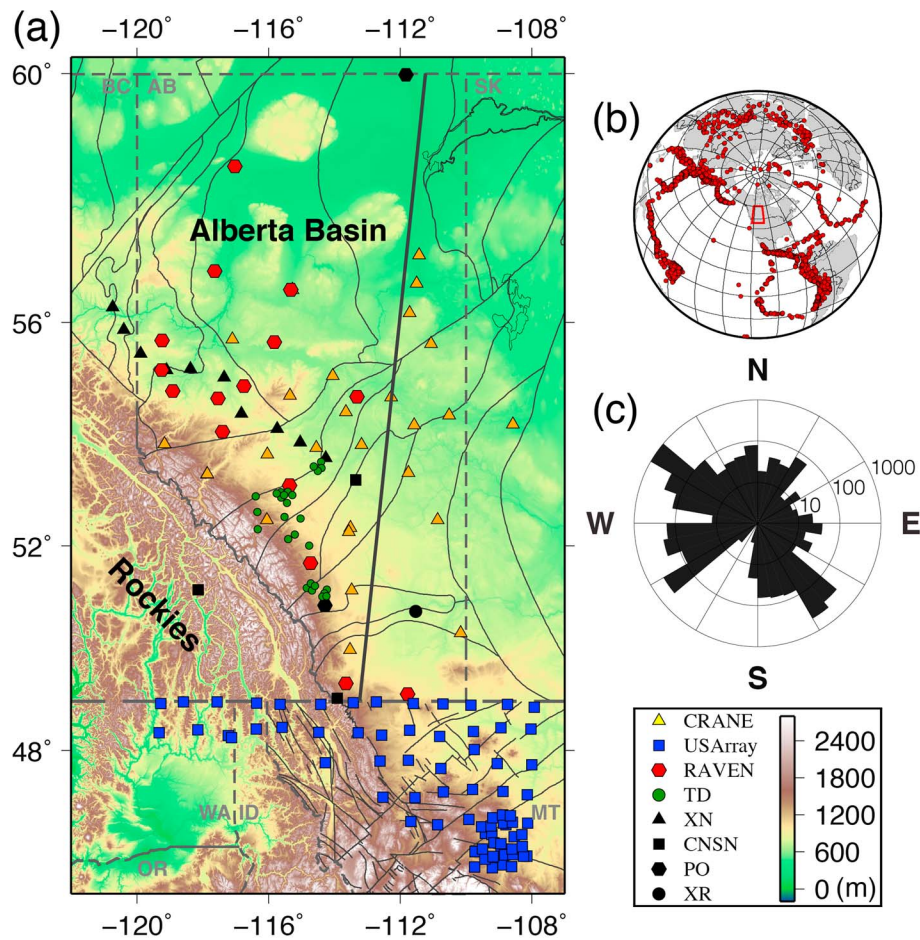


Figure 2. (a) Distribution of regional seismic stations examined in this study. The thin black lines indicate the tectonic boundaries within the Western Canada Sedimentary Basin and fault networks in northern Montana. The thick black line marks the location of a receiver function profile shown in Figure 4a. (b) Earthquakes (red circles) analyzed in this study. The study region is indicated by the red-colored polygon at the center of map. (c) A rose diagram (in logarithmic scale) showing the azimuth distribution of the earthquakes.

National Seismograph Network (CNSN; June 1991 to March 2015), 27 stations from CRANE (September 2006 to October 2015), 73 stations from USArray (mainly from 2008 to 2009), 27 stations from TD (July 2014 to July 2016), 15 stations from RAVEN (November 2013 to April 2017; Schultz & Stern, 2015) and 13 stations from temporal arrays (Figure 2a). A subset of this data that contains over 17,253 first arrivals was inverted for mantle velocities in a recent analysis of finite-frequency body wave tomography (Figure 3a; Chen et al., 2017). We also incorporate the results of ambient noise tomography (Gu & Shen, 2015; Figure 3b) for detailed comparisons. The data constraints on the GFTZ are primarily based on 73 stations from USArray, which were concurrent with several CRANE stations in Canada in 2007 and 2008.

The main contributions of this study are updated maps of Moho depth and crustal Vp/Vs ratios, which are determined from P-to-S converted wave at the Moho interface (P_{ms}) and its higher-order reverberations (Figures 3c and 3d). In comparison with travel times and dispersion curves, this data set offers greater constraints on the Moho depth, impedance contrasts, and composition, which are essential elements in the appraisal of potential boundary zones in western Laurentia. The main steps in processing this data set are presented in the sections below.

3.1. Receiver Function Calculation

We restrict our data set to earthquakes that occurred between 1991 and 2017 with moment magnitudes greater than 5.5 and epicentral distances ranging between 30° and 90° (see Figure 2b). These requirements are ideal for a receiver function (RF) analysis (Langston, 1977; Vinnik, 1977; Ammon, 1991; Rondenay, 2009),

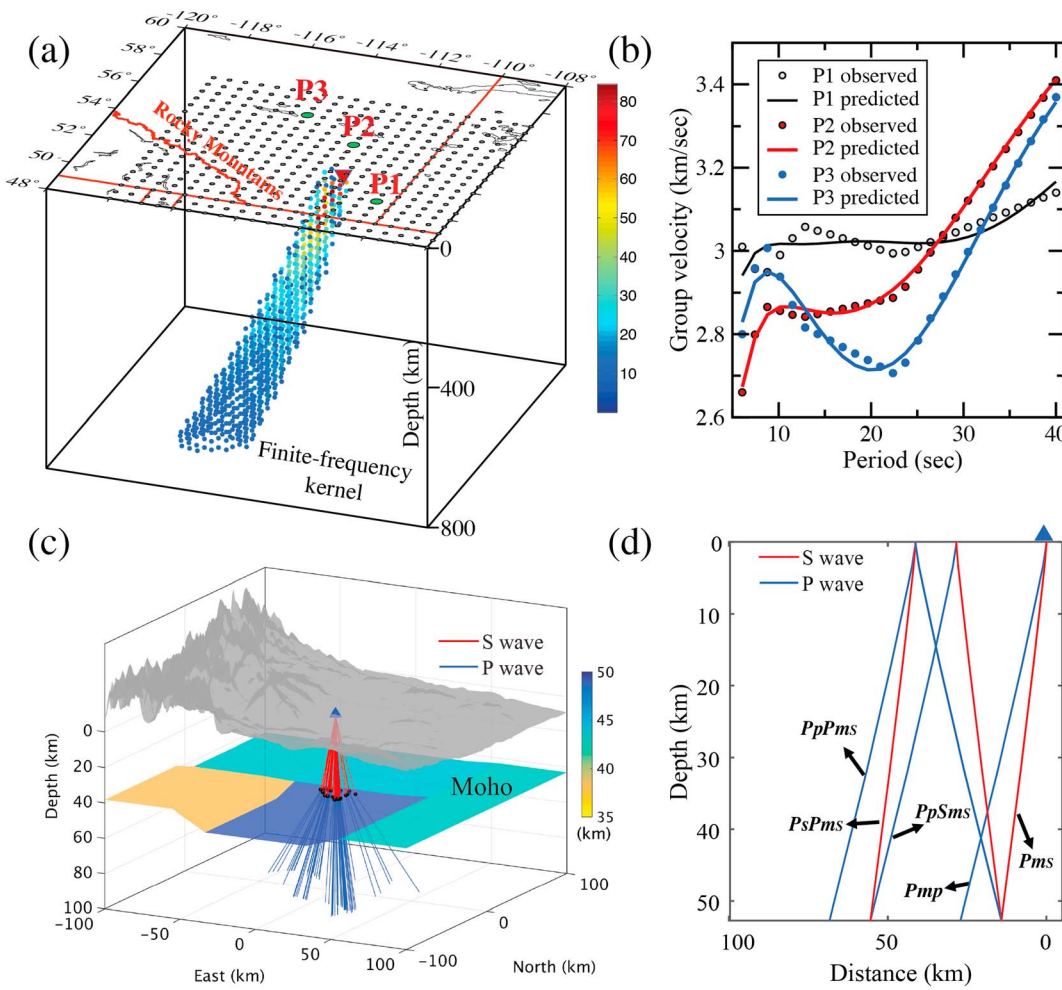


Figure 3. (a) Station-side finite-frequency kernels for shear velocity inversions, constructed using a teleseismic event at an epicentral distance of 85°. The circles show the inversion nodes where dispersion curves are computed from ambient noise correlation functions (Gu & Shen, 2015). Three nodes (green circles) are selected to show the sample dispersion curves (see Figure 3b). (b) Dispersion curves from selected nodes (P1–P3). The circles mark the observed group velocities at each period and the solid lines represent the predicted dispersion curves from 1-D shear velocity inversions (Gu & Shen, 2015). (c) A schematic diagram demonstrating the ray paths of P-to-S conversions beneath a station in the foothills. The conversion points are marked by the black circles on the Moho interface. (d) Ray paths of a direct P wave and four converted phases of a teleseismic event at an epicentral distance of 45° incident beneath a recording station. Compressional and shear waves are indicated using blue and red colors, respectively.

the main focus of this study, due to near-vertical incidence angles of the P wave ray paths. After the removal of instrument responses, we rotate the original components to vertical, radial, and transverse orientations, and subsequently apply a Butterworth band-pass filter with corner frequencies of 0.02 Hz and 3.5 Hz; this frequency range was empirically chosen based on experimentation to maximize the energy of the converted phases (Chen et al., 2015; Contenti et al., 2012). We then compute the standard deviation of the vertical-component seismogram in the time window of 1–25 s after the predicted P wave arrival time (Dziewonski & Anderson, 1981). The ratio between this value and that of the noise window, which is similarly defined for the time window of 105–5 s prior to P, is used as the signal-to-noise ratio (SNR) criterion to eliminate noisy records; we retain 19,085 (45% of the original data) high-quality source-station pairs with $\text{SNR} > 2$ for the analysis of RFs. The back azimuths of the station pairs favor a northwest-southeast orientation that precludes a comprehensive analysis of azimuth-dependent effects beneath most of the stations (Figure 2c).

The main imaging approach used in this study is RF based on P-to-S converted waves (Langston, 1977; Vinnik, 1977; Ammon, 1991; Cassidy, 1995; Bostock, 1996; Ligorría & Ammon, 1999; Gu et al., 2011; see Rondenay, 2009 for a detailed review). We compute RFs using the iterative time domain deconvolution technique of Ligorría and Ammon (1999) and an empirically determined Gaussian filter width of 2.5. Up to 400 iterations

are performed during the least squares minimization to ensure the convergence of the solutions, while a minimum 0.001% data fit improvement is imposed on each additional spike (Chen et al., 2015; Gu et al., 2015). The data misfit and percentage match to the original data allow further selection of the data set: RFs with a misfit greater than 20% are automatically rejected. This procedure improves the quality of the converted phases (rather than the dominant P phase), which yields 11,763 high-quality RFs for the subsequent processing. We then inspect each trace to further refine our data set and remove traces with weak Moho conversions or anomalously large reverberated energies; 10,043 traces are eventually retained after manual quality control.

3.2. H-k Stacking

To improve the crustal constraints, we simultaneously determine crustal thickness (H) and the ratio between P and S velocities (k) based on the H-k stacking method of Zhu and Kanamori (2000). This approach performs a grid search for the most energetic stack of the direct Ps phase and crustal multiples such as $PpPms$, $PsPms + PpSms$ based on predicted delays relative to the incident P wave (Zhu & Kanamori, 2000; Yeck et al., 2013; Figure 3d). We improve the stability and flexibility of Zhu and Kanamori (2000) further through a ray tracing-based approach (Niu et al., 2007) and a multilayer global crustal model (CRUST1.0; Laske et al., 2013). This implementation allows the inclusion of known regional structures such as sediment depth and crustal velocities beneath a given seismic station. Equal weights are applied to the three converted phases during energy stacking in view of the robust waveforms recorded by the majority of the stations (see Figure 5b). In comparison with a single-layer approximation, maximum energies from ray tracing-based approach generally agree to within 0.2 km in crustal thickness and 0.01 in Vp/Vs ratio. The ray tracing-based approach yields more coherent stacking energy in the H-k domain than the earlier approach, hence is adopted for the remainder of this study.

4. Result

4.1. General Assessment

With few exceptions, conversions from the Moho (i.e., Pms) are clearly detected at times ranging from ~5 s beneath the northern part of the array (e.g., FMC) to over 6 s beneath station CLA in southern Alberta. Conversions beneath the Alberta basin consistently arrive within 5 s relative to P (Figure 4a), which are 1–3 s earlier than those beneath the foothills of the Rockies. The time delays of Pms are accompanied by a notable amplitude drop-off near the foothills of the Rockies, where dipping Moho interfaces (Cassidy, 1992), sedimentation (Julià et al., 2004; Sheehan et al., 1995), and/or anisotropy with a nonhorizontal axis of symmetry (Levin & Park, 1997) could all contribute to scattering and defocusing. A relatively flat Moho in the Alberta basin results in clear converted phases (Figure 4b) and focused energy in the H-k domain (Figure 4c).

We compute the uncertainties of H and k (supporting information Table S1) using the bootstrap resampling method (Efron & Tibshirani, 1986) instead of the traditional derivative-based approach (Zhu & Kanamori, 2000). The uncertainties of Moho depth range from 1 to 4 km, showing an average of ~2 km. The average uncertainty of k is ~0.04, though values at certain stations (e.g., EDM, RW4) could be as large as 0.09. A further consideration is the uncertainty of average crustal P velocities in the region, as a perturbation of 0.1 km/s can cause a depth uncertainty up to 0.5 km. A pessimistic estimate of 0.4 km/s deviation from our assumed crustal velocities from CRUST1.0 model yields a depth error of ~2 km, which is considerably smaller than the key Moho gradients (5–10 km generally) detailed in the subsequent sections. The number of data traces (see Table S1 in the supporting information) and installation type (e.g., temporary versus permanent) do not appear to have major influences on the observed patterns. The stability of the measurements is best reflected by the outcomes of stations JOF and RDR (Figures 4d and 4e), which were installed on private farms that are 8.5 km and 4 years apart. The maxima of these two nearby stations are within 0.02 in Vp/Vs ratio and 0.4 km in Moho depth, well below the average uncertainty (~0.04 and ~2 km, respectively) in crustal property estimates.

While it is tempting to measure Moho properties exclusively using the H-k method, the outcomes are prone to severe errors in both crustal Vp/Vs ratio and Moho depth in the case of multiple energy foci in the H-k domain (Chen et al., 2010; Lowry & Pérez-Gussinyé, 2011; Zhu & Kanamori, 2000) due to crustal structural complexities. In our study region, a number of USArray stations in northern Montana show double or complex H-k maxima (e.g., station B19A, EGMT, C19A, D19A and D20A; see supporting information Figure S1).

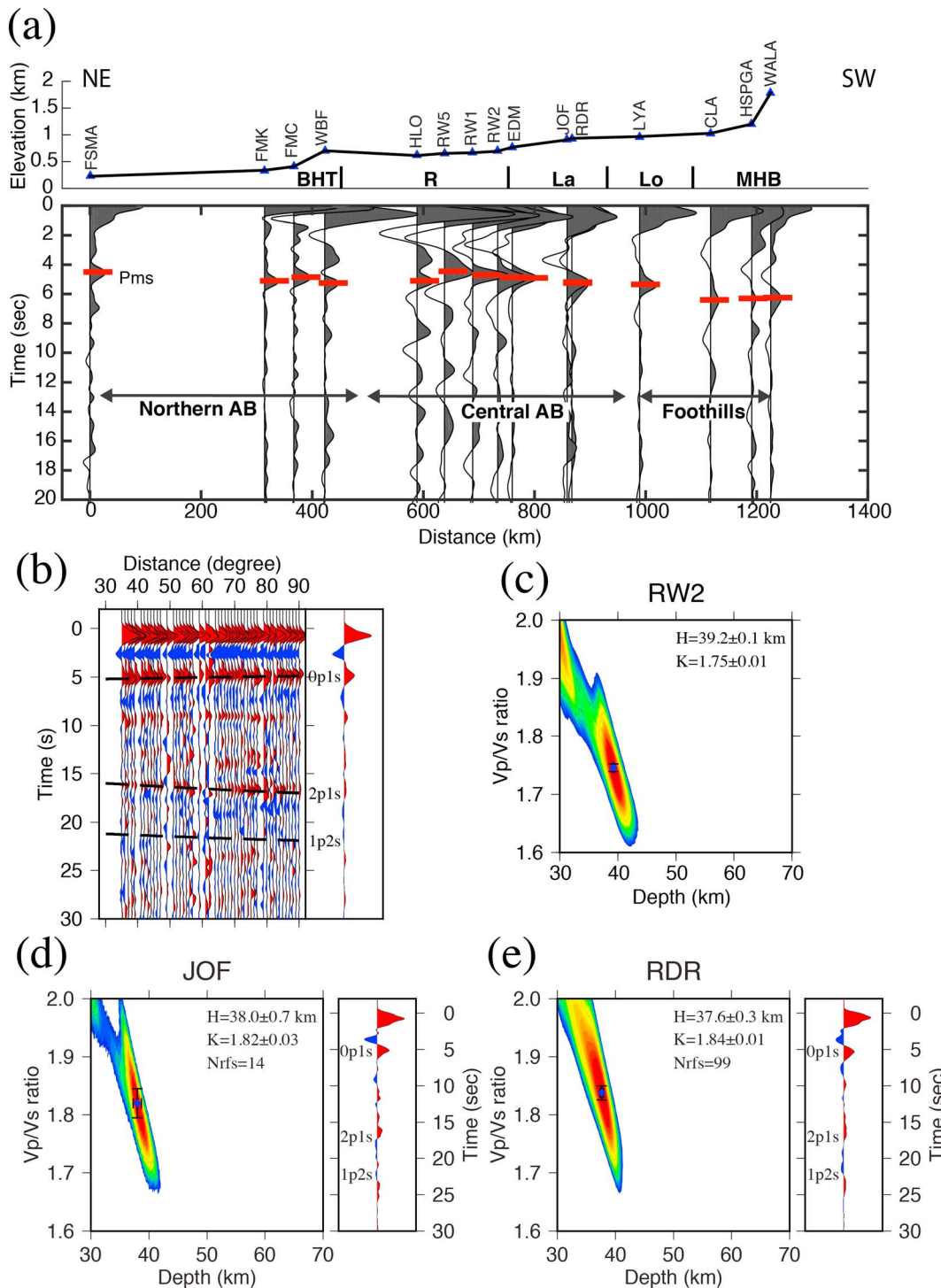


Figure 4. (a) A profile of stacked receiver functions (RFs) showing Moho variations from northern Alberta to the foothills of the Rocky Mountains (see Figure 2a for profile location). Station located within 50 km distance of the profile, which approximately equals the lateral resolution of the RF, are projected on the profile. The elevation and name of each station are indicated above the RF. The red line marks the P_{ms} phase. (b) RFs from station RW2. The dashed black lines mark the predicted arrival times of converted phases from H-k analysis. The stacked trace is shown on the right panel. (c) The H-k diagram of RFs from station RW2. (d and e) The H-k diagrams for two stations (JOF and RDR) that are 8.5 km apart. The stacked RFs are shown on the right-hand side.

Most of them reside within the region of early Proterozoic underplating (Clowes et al., 2002; Gorman et al., 2002) and present a major challenge to the evaluation and interpretation of true Moho depth; a detailed discussion of this important observation can be found in section 5. To mitigate crustal complexities and

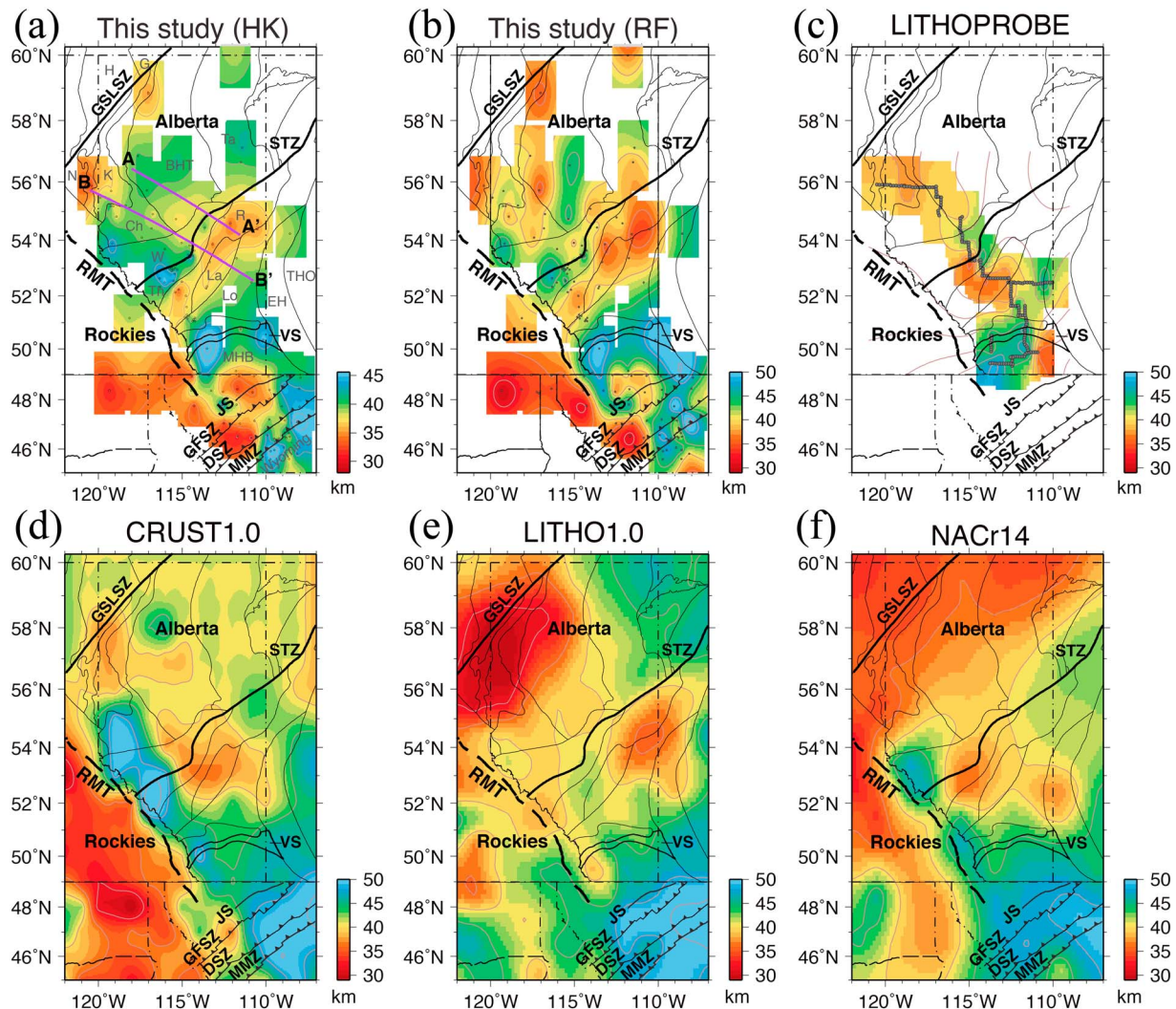


Figure 5. Maps of Moho depth from (a) H-k stacking (this study), (b) time-to-depth conversion (this study), (c) an interpolated map of Bouzidi et al. (2002) based on LITHOPROBE reflection/refraction surveys, (d) CRUST1.0 (Laske et al., 2013), (e) LITHO1.0 (Pasyanos et al., 2014), and (f) NACr14 (Tesauro et al., 2014) models. The locations of two linear transects across the STZ are indicated by the purple lines. The small gray circles indicate the locations of stations. Station elevation is subtracted from crustal thickness (H) to calculate the Moho depth.

verify the measured Moho depths based on H-k analysis (Figure 4), we convert the arrival times of P_{Ms} on the stacked RFs to Moho depths based on P and S velocities from CRUST1.0 (Laske et al., 2013). This approach assumes a near-constant Poisson's ratio of 1.75 from CRUST1.0, which is only an averaging approximation for the true crustal values, but the measured Moho depth is more resistant to anomalously large Poisson's ratios and multiple local H-k maxima.

The resulting Moho depths from transform and conversion-based approaches are highly consistent in regions with robust H-k signals, showing an average depth of ~40 km in the Alberta basin. Both maps contain a shallow Moho directly south of the STZ in the Alberta basin, which is identifiable in size and amplitudes to those of the processed sections from regional active-source surveys (Bouzidi et al., 2002, Figure 5c), global crust (CRUST1.0; Laske et al., 2013; Figure 5d), mantle lithosphere (LITHO1.0; Pasyanos et al., 2014; Figure 5e), or continent-wide (NACr14; Tesauro et al., 2014; Figure 5f) models. In contrast, a deep Moho is an essential fixture among all five models beneath the foothills of Rocky Mountains, particularly near the southern Canadian Rockies in the latitude range of 49–51°N (see Figure 5). Coupled with a flat, shallow (~35 km) Moho to the west of the Rocky Mountain Trench, this transition produces the steepest lateral Moho gradient in the study region. Part of this gradient could be attributed to an anomalously deep (~47 km) Moho beneath western segment of the VS. The anomaly is further evidenced by regional active source data (see Figure 5c),

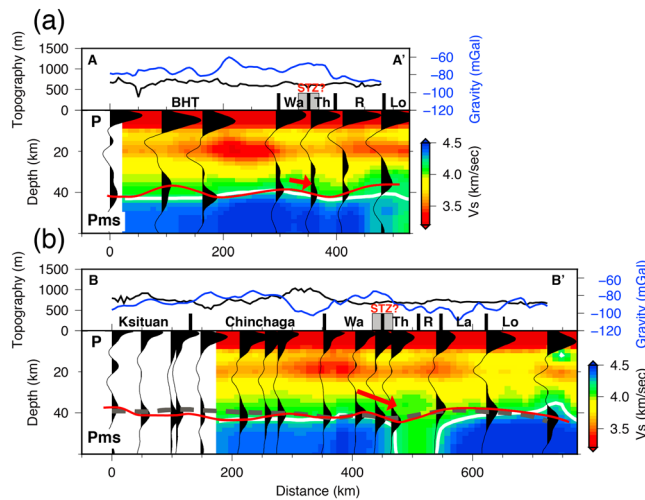


Figure 6. Two profiles of receiver functions in central Alberta showing the crustal structure variations across the Snowbird Tectonic Zone.

(a) Topography (black) and Bouguer gravity (blue) along the profile.
(b) Receiver functions (black) superimposed on shear velocities from ambient-noise tomography (Gu & Shen, 2015). The Moho determined from the P_{ms} phase and shear velocity (4.2 km/s contour) are highlighted using the red and white lines, respectively. The dashed black line represents the Moho depth from Bouzidi et al. (2002) based on LITHOPROBE reflection/refraction surveys. The red arrows indicate the orientations of Moho dip beneath the Snowbird Tectonic Zone. Domain name abbreviations are as follows:
BHT = Buffalo Head Terrane; Wa = Wabamun; R = Rimbe; Th = Thorsby;
La = Lacombe; Lo = Loverna block.

seismic perspective. Based on Figure 5, the Moho depth in central Alberta is divided into northwestern and southeastern halves, bordered by a crust that is 5–10 km thicker along the presumed southern strand of the STZ (Ross et al., 1993) than the regional average. This anomaly covers the entire Alberta section of the STZ, eventually merging with the deeper Moho along the eastern Talton Magmatic Zone in the northeast and terminating within the Cordilleran foreland belt in the southwest. The Moho depth ranges from 37 to 40 km south of the STZ, which are consistent with those reported by Bouzidi et al. (2002) within a spatially confined corridor of active source experiments (see Figure 5c). In comparison with CRUST1.0 (see Figure 5d), this zone of depressed Moho is much more significant along the STZ in our model (see Figures 5a and 5b).

Figure 6 carefully examines the Moho depths and crustal shear velocities along two semilinear transects roughly perpendicular to the STZ (see Figure 5a for profile locations). Along the easternmost transect (profile AA', Figure 6a), the Moho is significantly deeper beneath the BHT (by ~7 km) and the Thorsby (by 5 km) domains than beneath the STZ (~35 km). The latter anomaly is confined within the proposed boundary beneath the Thorsby domain, followed by a substantially shallower Moho beneath the Hearne province to the southeast. The Moho depth along the profile closely tracks the depth of a shear velocity of 4.2 km/s (white line, see Figure 6a), the average shear velocity between crust (~3.9 km/s) and mantle (~4.5 km/s, as defined in CRUST1.0; Laske et al., 2013), which we interpret as a gradational Moho interface due to inherent smoothing in noise correlation tomography (Gu & Shen, 2015). The first-order agreement between these two studies is highly encouraging, especially considering the substantially lower station spacing and data volume included in Gu and Shen (2015).

In transect BB', the Moho deepening beneath the Thorsby domain becomes more apparent, reaching the maximum regional depth of ~44 km (Figure 6b). This transect overlaps extensively with active-source lines 1–5 of the Central Alberta Transects of the LITHOPROBE project, where a sharp Moho depression of 5+ km was observed (dashed line, see Figure 6b) and interpreted as evidence for mantle faulting beneath the STZ (Bouzidi et al., 2002). The dimension and location of the Moho dip are consistent (see Figure 6) between these two studies despite different data frequencies and types. The interpreted average Moho depth based on

though its presence is only marginally supported (see Figure 5d) or unsubstantiated (see Figures 5e and 5f) in the remaining three Moho maps; we attribute these differences to insufficient resolution of global/continent-scale models. The RF stacks further suggest a deep Moho (~44 km) beneath eastern VS, resulting in an average Moho depth of 45.5 km along this east-trending geological structure (see Figure 5b). Unfortunately, we are unable to reliably resolve Moho depths in central VS due to the lack of local seismic stations.

Farther south, the Moho deepens toward the southeastern corner of the study region in northern Montana in all models (see Figure 5). Unlike northern MHB in southern Alberta, where the Moho exceeds 45 km (in most models), our receiver-function based results show significantly shallower Moho directly north of the GFSZ than the earlier studies (see Figure 5a). This observation is supported by the outcomes of both H-k stacking and depth converted RFs, regardless of the presumed V_p/V_s ratios of ~1.84 and ~1.74, respectively. There are other notable differences among the various crustal depths shown in Figure 5: for example, the scales of the anomalies in our maps are generally smaller than those in the earlier studies, which we attribute to increased lateral resolution due to improved station coverage from regional broadband arrays. The sections below mainly focus on the characteristics of the Moho near the STZ and GFTZ, the two best constrained geological structures by our regional data set.

4.2. Crust and Mantle Beneath the STZ

The combined station coverage from regional networks allows us to examine crustal imprints and lateral dimensions of the STZ from a broadband

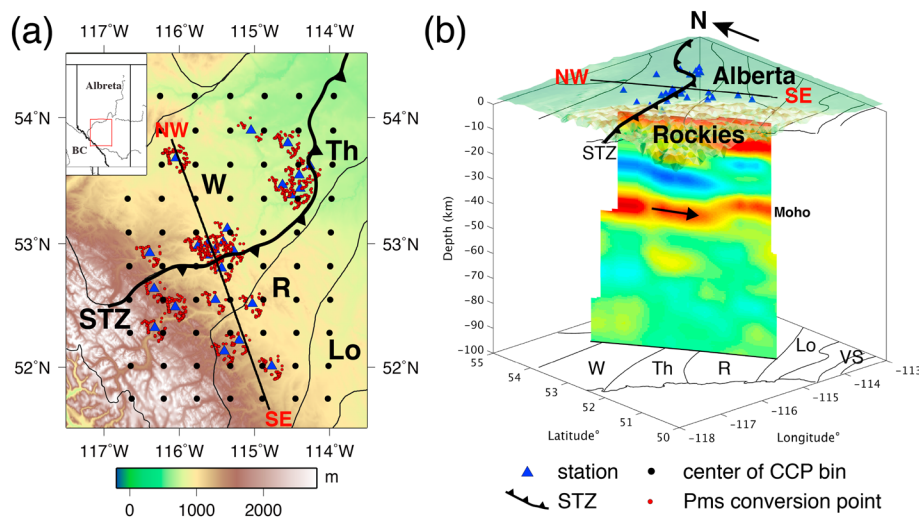


Figure 7. (a) A tectonic map of western Snowbird Tectonic Zone (Ross et al., 1993). The blue triangles mark the seismic stations used in the construction of common conversion point (CCP) gathers. The black circles indicate the centers of the CCP bins, and the red circles denote the P -to- S conversion locations at 40-km depth. The black line shows the location of the receiver function transect. The map area is shown by the enclosed region in the inset. (b) A 3-D perspective plot of the receiver function transect extracted from the CCP gathers. Red and blue colors represent the positive and negative amplitudes, respectively. The Moho is delineated by a positive (P_{ms}) phase at \sim 40-km depth, and its dipping direction beneath the Snowbird Tectonic Zone is indicated by the arrow.

shear velocities (42.3 km) in the overlapping areas fits within the RF estimate (41.5 km) from this study. In the vicinity of Thorsby/Rimbey domain, the location of the Moho dip, we observe substantially reduced mantle shear velocities down to a minimum depth of 60 km. The significance of which will be discussed in conjunction with similar observations near the GFTZ in section 5.

Taking advantage of the recently installed TD array (see Figure 2a), which was designed predominantly to increase local receiver densities for microseismicity monitoring, we are able to resolve the Moho topography across the STZ with greater clarity using the common conversion point (CCP) stacking technique (Dueker & Sheehan, 1997; Rondenay, 2009; Levander & Miller, 2012). The CCP volume is constructed using over 2000 RFs from 25 stations near the STZ (Figure 7a). Each RF is migrated to depth using AK135 (Kennett et al., 1995) and corrected for local heterogeneities based on CRUST1.0 (Laske et al., 2013) while assuming a fixed ray path. Each CCP gather is a stack of RFs with conversion points that fall within a common bin, and the distance between bins is controlled by the width of the Fresnel zone (Červený & Soares, 1992). Considering a dominate frequency of 1.2 Hz and average crustal shear velocity of \sim 3.45 km/s, the width of the CCP profile is about 15 km at 40 km depth (Ryberg & Weber, 2000), which defines the maximum horizontal resolution of the CCP image. It is worth noting that due to irregular station distribution and incomplete azimuthal ray coverage, the maximum achievable resolution is usually significantly less in practice. We set the bin spacing to 30 km, which approximately equals the station spacing in the center of the imaging volume (Figure 7a). We apply spatial smoothing to the CCP image using a 40-km running average window to minimize imaging gaps and improve the coherences of converted energy (Frassetto & Thybo, 2013). The resulting stacked RFs provide further evidence of a \sim 50-km wide Moho deepening (Figure 7b). This anomaly initiates near the northern boundary of the Thorsby domain, as evidenced by the depth gradients in both the Moho conversion and the negative phase preceding it, and eventually terminates in the vicinity of southern Rimbey domain where (1) the Moho surface raises by \sim 8 km toward the south and (2) the conversion amplitude decreases due to nonplanar structures.

To explore the depth extent of the STZ, we carefully examine the mantle shear velocities extracted from S wave finite frequency tomography (Figure 8; Gu et al., 2016). This model takes advantage of the most up-to-date regional array data and the inversion considers the volumetric sensitivity of seismic waves to the mantle structure (Hung et al., 2004). Based on standard “checkerboard” test (supporting information Figure S2), the nominal lateral resolution is sufficient to resolve the structure around the STZ in central Alberta. Our shear velocity model shows distinctive high-velocity clusters beneath the Wabamun domain and Hearne craton (Figures 8a and 8b), separated by a low-shear velocity zone that extends down to \sim 80 km depth.

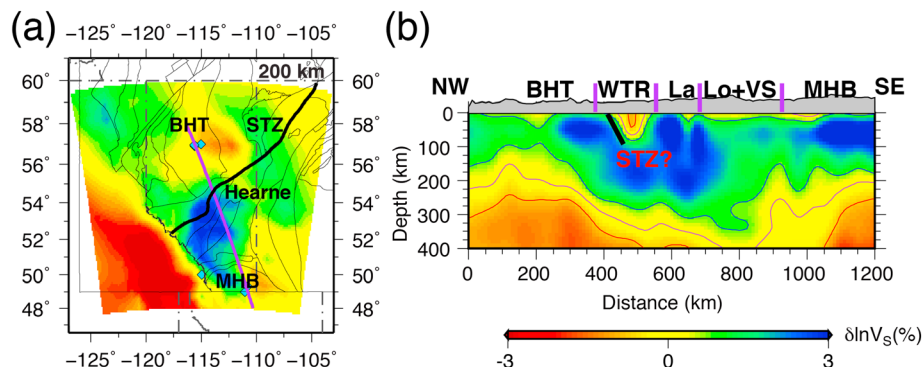


Figure 8. (a) Shear velocity perturbations at 200-km depth from finite-frequency travel time tomography (Gu et al., 2016). The blue diamonds show the location of xenoliths (Buhlmann et al., 2000; Canil et al., 2003; Aulbach et al., 2004). (b) A cross-section of shear velocity profile. Its location is indicated by the purple line in (a), and the potential subsurface extension of the Snowbird Tectonic Zone is indicated by the thick black line. The domain boundaries are marked by the purple lines near the surface. WTR represents the region across the Snowbird Tectonic Zone that includes the Wabamum, Throsby, and Rimbeay domains. See Figure 1 caption for other abbreviated domain names.

4.3. Moho and Shallow Mantle Structure Beneath the GFTZ

In comparison with northern central Alberta, the Moho is generally deeper beneath southern Alberta and northern Montana, showing an overall average of 42 km in this study (see Figure 5a) and 46 km in CRUST1.0 (Laske et al., 2013; see Figure 5d). The most significant dip is observed in the southeastern corner of the study region, reaching ~50 km beneath the DEEPPROBE active source profile (Clowes et al., 2002; Figures 9a and 9b). At 48°N in northernmost Montana (Figure 9b), the Moho depth increases sharply from 40 km to ~50 km along the eastern provincial boundary of Alberta. The position of this anomalous dip roughly overlaps with the proposed LCL structure (Gorman et al., 2002), which was later supported by broadband seismic analyses using RFs (Levander & Miller, 2012; Gilbert, 2012; Schmandt & Lin, 2014). This east-west Moho gradient is notably absent in global crustal models (e.g., CRUST1.0; Laske et al., 2013; see Figure 5d), however.

Figures 9c–9e showcase three cross-sections of depth-converted RFs parallel to the DEEPPROBE line (Clowes et al., 2002; Gorman et al., 2002) in northern Montana. The depths of the Moho along these transects, which are expected to intersect the GFTZ at progressively greater offsets from the northeast, shed further light on the robustness of this proposed suture zone between the MHB and the Wyoming craton. In all three cases, the Moho exhibits shallow depths beneath the MHB northwest of the boundary, but deepens substantially below the DSZ and MMZ. The positions of the Moho dip are generally consistent among published regional studies based on broadband data (see Figure 9). All three transects across the GFTZ contain a weak seismic arrival prior to P_{ms} and its corresponding station location roughly overlaps with the region of the proposed Proterozoic underplating (Clowes et al., 2002; Gorman et al., 2002). This arrival is further evidenced by multiple energy peaks in the H-k domain (see supporting information Figure S1).

This sharp gradient in Moho depth runs progressively southward (Figure 10a) and overlaps with a broad aeromagnetic low south of the GFSZ (Sims et al., 2004; see Figures 10a and 10b). This Moho anomaly extends to the southeast of the LBM (see Figure 10a, cross-section DD'), where significant earlier Proterozoic signatures were identified based on geological and geochemical data (Mueller & Frost, 2006). The overall correlation between potential field and Moho depth is low in the study region; for example, the Moho is flat beneath the two sharp northeast trending potential field gradients along the JS and GFSZ in the northernmost Montana (Figures 10b and 10c).

5. Discussion

This study presents new broadband seismic observations on the continental crust beneath the western margin of the North American craton. While resolution remains a work-in-progress beneath parts of the WCSB, especially along northeastern MHB, the seismic observations from regional broadband array presented in this study are the most substantial to date and offer new constraints on the tectonic development and crustal processes. The updated data and models enable an unbiased appraisal of the existing theories based largely on potential field and active source data.

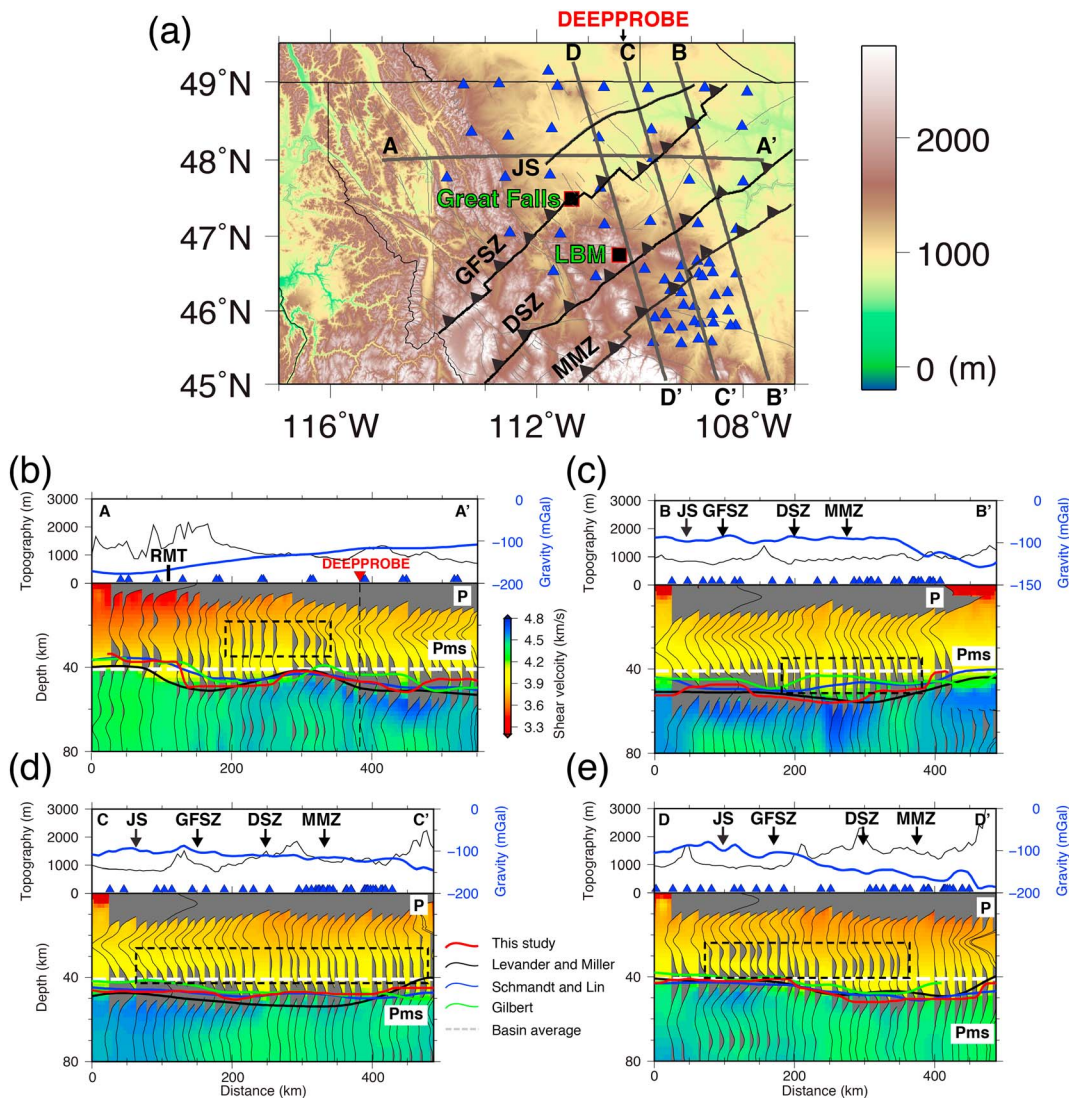


Figure 9. (a) Surface topography near the Great Falls Tectonic Zone in northwestern United States. The blue triangles mark the station locations, and thin black lines indicate four major northeast orientated faults. (b–e; top) Topography (black) and Bouguer gravity (blue) along the profiles shown in (a). The intersections between known faults and seismic profiles are highlighted by the arrows. (bottom) RF transects constructed from the CCP gathers. The background color shows the shear velocities from Shen and Ritzwoller (2016). The solid lines track the Moho depth obtained from this (red) and earlier (Gilbert, 2012; Levander & Miller, 2012; Schmandt & Lin, 2014) studies. The averaged Moho depth in the Alberta basin is shown by the white dashed line. In general, stations with delayed, high-amplitude Moho conversions are underlain by above-average shear velocities. The stacked traces from these stations often show waveform broadening or multiple arrivals (enclosed by the dashed rectangles).

5.1. General Appraisal of Existing Models of Moho Depth and Composition

Despite the wide range of adopted data constraints, the proposed depths of the Moho beneath the WCSB, the bulk of the study region, are generally correlated among various studies (see Figure 5). Prime examples are the Alberta basin, northwestern Alberta, and Cordillera, beneath which the Moho is consistently shallower (i.e., thin crust) than the regional averages. This is supported further by earlier findings from RFs at a few select locations (Eaton & Cassidy, 1996; Gu et al., 2011; Shragge et al., 2002). Sprinkled in between are areas of deep Moho (thick crust), for example, beneath the foothills of the Rockies, most notably in western Wabamun domain and VS/MHB. The most notable differences among the various studies are the amplitudes and resolutions of the major anomalies in the WCSB. For example, due to the use of regional stations, our maps show significantly greater details on Moho depth (see Figure 5) than previous published models that were derived from limited active-source data (CRUST1.0) or surface waves (LITHO1.0). Furthermore, the transition from the Alberta basin (thin crust) to the foothills (thick crust) is sharper in our model than in LITHO1.0, which we partly

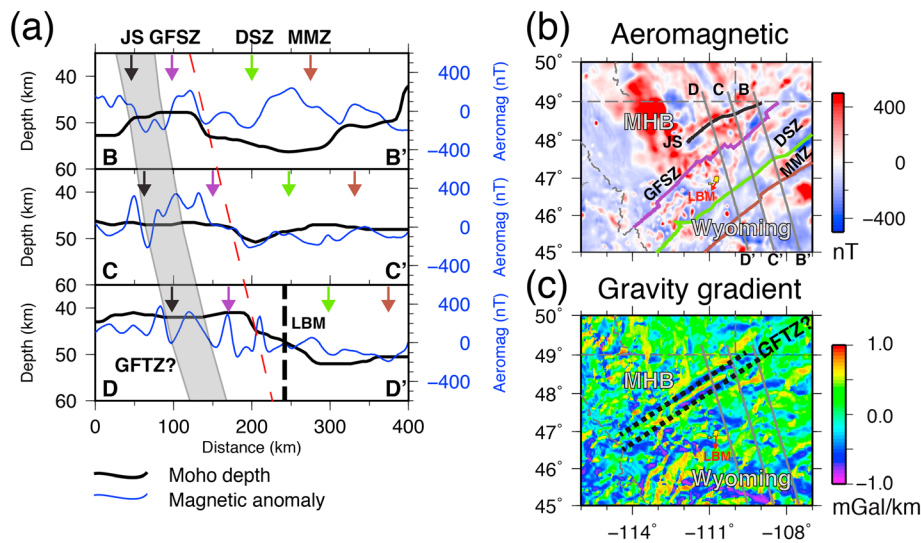


Figure 10. (a) Moho depth along three profiles that traverse the Great Falls Tectonic Zone (GFTZ). The intersections between the profiles and faults are indicated by the arrows. The shaded region indicates the location of the GFTZ defined by the gravity gradients shown in (c). The red dashed line marks the onset of crustal thickening. (b) Aeromagnetic anomalies near the GFTZ. Three sample cross-sections are marked by gray lines, and faults are delineated by thick lines in various colors. (c) Normalized gravity gradients near the GFTZ. The GFTZ is originally defined as a narrow zone between the two parallel, negative gravity gradient lineaments (dashed lines) in northern Montana (e.g., Clowes et al., 2002; Gorman et al., 2002); this definition is challenged by the results of this study.

attribute to the effects of damping/smoothing in the earlier global model due to spatial undersampling within the WCSB. Differences aside, the Moho depth measurements of the WCSB do not appear to be strongly affected by the data type (i.e., active-source versus broadband).

A similar conclusion cannot be reached for the crustal structures in northern central Montana, however. The average Moho depth determined from USArray data by our study (~45 km; see Figure 5 for map and Figure 9b for E-W cross-section) is nearly 5 km shallower than those from maps that relied heavily on the active-source data (see Figure 5d). A part of this discrepancy could be attributed to fewer surface seismic surveys (e.g., mainly along a linear DEEPPROBE transect) in comparison with the WCSB, which adversely affected the lateral resolutions of the existing global crustal models such as CRUST1.0 and LITHO1.0. Complexities associated with complex crustal structures (e.g., underplating and mantle intrusion), which are reflected in the differences (~6 km) between H-k (see Figure 5a) and time-to-depth conversion (see Figure 5b) methods, will be explored further in the following sections.

5.2. Implications for the STZ

Of all the broadband seismic observations examined in this study, a deep Moho is the most compelling observational constraint for the presence of the STZ across the WCSB. Supported by migrated RFs (see Figure 7), the deep Moho overlaps with the earlier report of a 10 km Moho step associated with a high-angle fault (Bouzidi et al., 2002). Similar crustal thickening has been documented near Rae-Chesterfield in eastern STZ and interpreted as a consequence of subduction circa 1.9 Ga (Berman et al., 2007). While the timing and process of crustal thickening in western STZ remains debated due to the scarcity of geological samples, collisional tectonics certainly offer a simple and compelling explanation supported by other observational constraints. For instance, a thick crust beneath the Thorsby basin (presumed Proterozoic suture; Ross et al., 1993) is compatible with the lower-than-average value of Bouguer gravity in the vicinity of the STZ. Formerly known as Edmonton-Kasba low (e.g., Bouzidi et al., 2002; Ross et al., 1991), a gravity anomaly (see Figure 6) was identified slightly south of the depressed Moho near the Thorsby domain in central Alberta. While its clarity and linearity are highly dependent on (1) the processing method and (2) structural complexities (e.g., nearby fault or intrusive sill; Pana, 2003), a thick and low-density crust could certainly contribute to a reduced Bouguer gravity value.

Seismological expressions of the STZ are evident in crust (Gu & Shen, 2015) and mantle (Chen et al., 2017) shear velocities. In both studies, a distinctive low shear velocity zone is present in the lower crust-upper mantle beneath Thorsby/Rimbey domain (see Figure 8b). Sandwiched between two distinct high-velocity

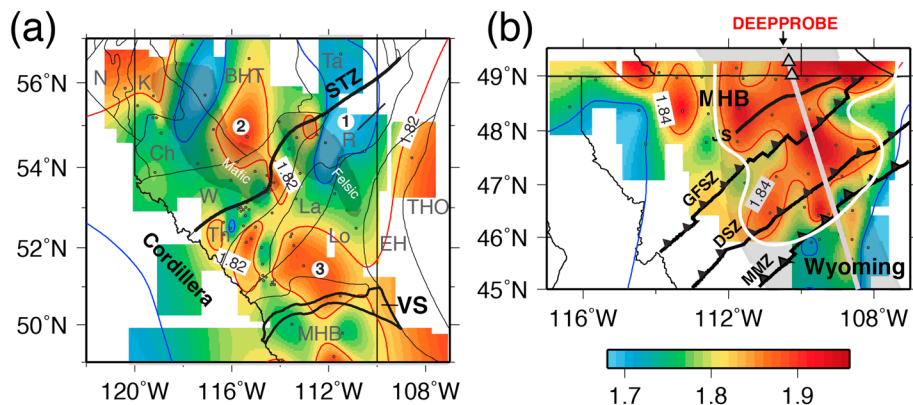


Figure 11. Vp/Vs ratios near the (a) Snowbird Tectonic Zone and (b) Great Falls Tectonic Zone. Labels 1–3 highlight the major anomalies. The DEEPPROBE refraction transect and shot points (Henstock et al., 1998; Gorman et al., 2002; Clowes et al., 2002) are indicated by the white line and grey triangles, respectively. The shaded areas show the reported mafic and felsic magmatic intrusions from earlier geophysical studies (Bouzidi et al., 2002; Chen et al., 2015; Ross, 2002; Ross & Eaton, 1997; Welford & Clowes, 2006). The region of underplating (i.e., lower crustal layer) inferred from elevated Vp/Vs ratios is enclosed by the white line.

zones, which were interpreted as the cratonic roots of the Archean Hearne province and BHT (Chen et al., 2017), this low-velocity zone is symptomatic of a possible tectonic suture (Porritt et al., 2014; Youssouf et al., 2015). The steep basal relief on the mantle lithosphere, which produces a major structural gradients across the cratons (Chen et al., 2017), may be further evidence for a plate boundary if the difference between basement domains extends vertically down to lithospheric depths (see Figure 8).

Further insights on the crustal composition and the existence of potential suture zones could be gained from Vp/Vs ratios (Christensen, 1996; Niu et al., 2007; Zandt & Ammon, 1995; Zhu & Kanamori, 2000). We construct a Vp/Vs ratio map using the H-k results from this study in combination with earlier measurements from five stations (Table S1) in southern Alberta (Shragge et al., 2002; Figure 11a). The entire STZ is divided into two distinct segments, a western central Alberta segment with four distinct clusters of high (>1.82) Vp/Vs ratios and a northeastern segment embedded within an elongated, north-south oriented belt with below-average (<1.73) values (see zone 1 in Figure 11a). The former observation could be linked to a suture, where arc magmatism and intrusion of mafic mantle melt may have transpired during the subduction of the Thorsby domain circa 1.8 Ga. Similar observations have been made in various collisional zones globally (e.g., Yuan et al., 2000; Darbyshire et al., 2017). This cluster of enhanced Vp/Vs values is interrupted in eastern central Alberta near the Talton Magmatic Zone, a proposed Proterozoic (2.02–1.91 Ga) orogen between the Slave and Superior cratons (2.3–2.0 Ga, Ross et al., 1991; Boerner et al., 2000). As potentially a southern segment of the Thelon orogen (Hoffman, 1988; Ross & Eaton, 2002; De Suman et al., 2000; Berman et al., 2007), the Talton Magmatic Zone has been linked to Paleoproterozoic collisions and the presence of medium-to-high pressure microdiamond (Berman et al., 2007). Further geochemical analyses of granitoids (De Suman et al., 2000) suggest the Thelon-Talton belt to be akin to felsic, intra-continental mountain belt similar to Tian Shan in central Asia (Chacko et al., 2000; De et al., 2000). Based on our RF H-k analysis, the Vp/Vs values (~ 1.70) are consistently low beneath the Talton Magmatic Zone, which corroborates the earlier findings based on isotopic data. It is worth noting that below-average Vp/Vs ratios are also observed directly south of the STZ, overlapping an earlier reported zone of high heat flow and low crustal shear velocities (see Figure 11; Chen et al., 2015). Anatectic melting in response to the tectonic vise model may be responsible (Chen et al., 2015, 2017).

Enhanced Vp/Vs ratios in the Wabamun/BHT (zone 2 in Figure 11a) and southern Alberta (zone 3 in Figure 11a) have further implications for Precambrian tectonics. Extensive intrusive sills have been discovered in the former region, which manifest into thin, high-velocity reflective layer known as the “Winagami reflection sequence” (Chen et al., 2015; Ross & Eaton, 1997; Welford & Clowes, 2006). The origin and precise age of these sills remain unclear, but it is highly probable that their existence required the participation of the ultramafic upper mantle. A similar argument could be made regarding the crustal composition south of the STZ, where a low-resistivity zone known as the “Red Deer conductor” has been identified and linked to a north dipping subduction zone beneath the VS by a recent magnetotelluric survey (Nieuwenhuis et al., 2014). Further discussion of this southern Alberta anomaly is given in section 5.5 in connection with the VS.

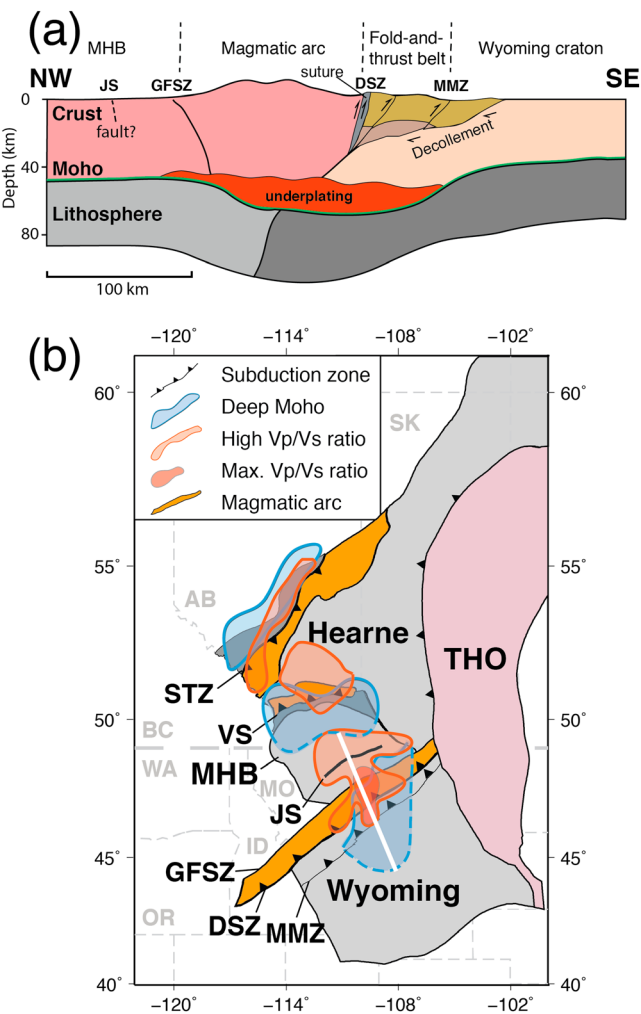


Figure 12. (a) A schematic cross-section showing the mechanisms of crustal thickening near the Great Falls Tectonic Zone (GFTZ). The location of the profile is shown by the white line in (b). The crust could be thickened by arc magmatism, arc-continent collision, load of the fold-and-thrust belts and magmatic underplating. Note that the Joplin Structure (JS), originally defined as the northern boundary of the GFTZ, does not show a significant increase in Moho depth and likely represents an intracontinental structure. (b) A map showing the Hearne-MHB-Wyoming (HMW) tectonic system, which is featured by contemporaneous (2.0–1.8 Ga) subductions, continent-continent collisions, and the associated magmatic events on the western margin of Laurentia. Superimposed regions with a deep Moho (blue contours) and high Vp/Vs ratios (red contours) are selected based on threshold values of 38 km and 1.82, respectively, near the Snowbird Tectonic Zone (STZ). The corresponding contour values near the VS and GFTZ are 40 km and 1.84, respectively. The dashed contour indicates questionable boundaries of deep Moho due to insufficient data.

shear zones in the hinterland of the TMO formed during the Paleoproterozoic collisional events. This interpretation is corroborated by (1) a flat Moho across the JS (see Figures 9c–9e), which suggests predominantly strike-slip motion and/or limited depth extension, and (2) the apparent lack of magmatic signatures in the magnetotelluric data in the presumed Canadian segment of the GFSZ (Boerner et al., 1998).

Details of cross-sections of RFs along the GFTZ enables a reexamination of other proposed tectonic processes in the study region (Figure 12a). First, aside from anomalously high values (~1.90) near the LBM (see Figure 11b), which may be associated with the aforementioned Paleoproterozoic magmatic processes,

5.3. Location and Crustal Origin of the GFTZ

RFs offer new geophysical constraints on the tectonic history of the MHB and northern Wyoming province. Similar to the STZ, a characteristic depression on the Moho interface is identified in the vicinity of the LBM (see Figures 9 and 10a), one of the few exposed locations with solid geochemical evidence for Proterozoic overprinting (1.9–1.8 Ga; Mueller et al., 2002). We interpret this observation as new seismological support for the existence of the Wyoming-MHB collisional suture. While crustal thickening can result from a wide range of processes (Haschke & Günther, 2003; Thybo & Artemieva, 2013; see section 5.5), Paleoproterozoic plate convergence between the MHB and northern Wyoming province offers a simple mechanism consistent with the earlier-proposed tectonic framework of western Laurentia (Mueller & Frost, 2006; O'Neill & Lopez, 1985; Ross et al., 2000). The zone of deep Moho coincides with the Trans-Montana Orogen (TMO; Sims et al., 2004; see Figures 5a and 9), which is terminated by the THO (~1.8 Ga) in the east and the transitional crust of Mesozoic-Paleozoic in the west (O'Neill, 2007). The onset of this crustal anomaly resides ~50–100 km northwest of the DSZ (see Figures 9c–9e and 10a), a proposed suture zone during the Paleoproterozoic collision, and the southern edge of this anomaly (near MMZ) appears to be an integral part of the fold-and-thrust belt of the TMO (O'Neill, 2007; Sims et al., 2005, 2004).

Since the first report of the GFTZ based largely upon observations of a northeast trending major fault system (O'Neill & Lopez, 1985), the detailed characteristics and origin of the Wyoming-MHB collisional suture have caused considerable confusion in the literature. Questions have surfaced regarding both the location (Clowes et al., 2002; Hoffman, 1989; Mueller et al., 2002; Sims et al., 2004) and the age (Proterozoic versus Archean) of the suture (Clowes et al., 2002; Gorman et al., 2002; Whitmeyer & Karlstrom, 2007). With limited geological sampling this suture is often quantified as (1) a narrow structure confined between the JS and GFSZ, two potential field gradients (Clowes et al., 2002; Gorman et al., 2002; see Figure 10c), or (2) a broad, hundreds-of-kilometer-wide (Sims et al., 2004, 2005) geological structure demarcated by the GFSZ as its northwestern boundary. The crustal observations from this study are able to refine the boundary zone definition and make important inferences. First, there is the clear spatial separation (by ~200 km) between the northeast trending crustal thickening under DSZ (see Figures 9c–9e) and the potential-field gradient zone near the JS (see Figure 10). The Moho anomaly coincides with Paleoproterozoic magmatic belt and the foreland region of the TMO based on geological evidence of thrust sheets (Sims et al., 2004), despite the absence of present-day surface elevations. Its tectonothermal origin is reinforced by a sharp increase of Vp/Vs ratios that potentially resulted from mafic mantle intrusions (Figure 11b). On the other hand, the Joplin potential field anomaly (which coincides with the JS) and extensive fault systems of GFSZ ~50 km to the southeast were likely the ductile

Vp/Vs ratios throughout northern Montana (1.84) are generally higher than the southern Alberta (1.75–1.80, see Figure 11a). The elevated Vp/Vs ratios could reflect widespread mantle intrusions, hence increased average crustal mafic content, due to either Paleoproterozoic intrusions or the reactivation of the extensive network of basement-controlled faults near the GFSZ since then (Sims et al., 2004). Furthermore, we detect a potential weak reflector that coincides with the Moho dip (see Figure 9), which spatially overlaps with the earlier-proposed high-velocity, underplated Proterozoic layer (Gorman et al., 2002; Clowes et al., 2002; Levander & Miller, 2012; see Figure 12a). The presence of this layer is further suggested by recent models of shear velocities (Shen et al., 2013; Shen & Ritzwoller, 2016; see Figure 9), despite moderate differences between Moho depth deduced from our RF analysis (45–50 km), and values along the DEEPPROBE profile suggested by Gorman et al. (2002; 50–60 km). This anomalous lower crustal layer has been recently examined through RF simulations (Schulte-Pelkum et al., 2017), and factors such as (1) lower depth resolution in broadband RFs and (2) inaccuracies during the depth migration of active-source data could have contributed to the systematic difference (~10 km) among these studies. It is nonetheless encouraging that a lower crustal reflector, a deep Moho interface, and enhanced lower crustal/shallow mantle seismic velocities at the base of the crust are self-consistent with an underplated high velocity LCL. The inferred dimensions of this potential LCL also highlight considerable departures between our observations (see Figure 12a) and findings based on active-source data. For example, Clowes et al. (2002) reported a flat, thick (>10 km) LCL and very weak seismic signatures directly associated with the Wyoming-MHB suture (Gorman et al., 2002). Their anomaly initiates from the southern MHB and continues southward across the GFTZ to the southern Wyoming craton (see Figure 11b), extending over a distance of more than 600 km. The widespread lower crustal conversions support a relatively broad LCL surrounding the DEEPPROBE transect (e.g., Ross, 2002). However, judging from the localized deep Moho and sharp termination of the Vp/Vs ratio along the MMZ, the LCL is clearly confined to a northeast striking zone no wider than 300 km in the TMO (see Figures 11b and 12a); that is, the north-south extent of the LCL is considerably smaller than earlier suggested (see Figures 1c and 11b). The affinity of the crustal anomaly to the TMO based on RFs is compelling support for the more recently proposed spatial location of Trans-Montana orogeny (Mueller & Frost, 2006; Sims et al., 2004, 2005), as well as its defining role, during Paleoproterozoic plate convergence.

5.4. Potential Mechanisms for Crustal Thickening

Arc magmatism at convergent margins is an effective process for crust thickening and differentiation (Haschke & Günther, 2003). There are certainly parallels between the STZ and GFTZ, where subduction of ocean basins (Thorsby and Wallace oceans, respectively) preceded continent-continent collisions (Ross et al., 1991; Sims et al., 2005). During the first stage of the collisional process, the crust beneath the continental domains thickens through a wide range of mechanisms. Based on data compiled from global subduction zones, Karlstrom et al. (2014) highlights the critical roles of arc magmatism in both arc front migration and crustal thickening of the overlying continental plate. Intrusion of mantle melts from the dehydration of hydrous minerals can thicken subarc crust through (1) magmatic underplating at the base of the crust (e.g., Haschke & Günther, 2003; Thybo & Artemieva, 2013), (2) intercrustal thickening and chemical differentiation, and (3) surface generation of new continental crust via arc volcanism (Stern et al., 2002; Karlstrom et al., 2014). All three mechanisms may have commenced during the early Proterozoic, contributing to a thick crust in a similar fashion as the present-day crustal growth landward of the Juan de Fuca subduction zone (Bostock, 2013; Calvert et al., 2006). It has been suggested that following the completion of oceanic subduction during the early Proterozoic (Ross et al., 1993, 2000; Sims et al., 2004, 2005), continent-continent subduction became the dominant tectonic process along both the STZ and the GFTZ. During this later stage of plate convergence, tectonic thickening likely occurred, resulting in further crustal growth beneath the orogenic belts near the collisional boundaries. The overthrusting occurs in zones with high strain concentration and forms foreland-verging structures (Godin et al., 2006), which could have created the downward flexure of lithosphere due to the mass load (Beaumont, 1981; see Figure 12a). The style of convergence and crustal thickening could be comparable to those beneath the Zagros mountain belt formed during the collision between Arabian and Eurasian plates (Paul et al., 2006; Pirouz et al., 2017), South American Andes (Haschke & Günther, 2003) and the Paleoproterozoic THO (directly east; Weller & St-Onge, 2017). While the fractional crustal growth from various mechanisms during these Proterozoic

collisional episodes remains unclear without further constraints, the total crustal thickness has been suggested to reach 55 km in both the STZ and GFTZ at their time(s) of formation (Barnhart et al., 2012; Bouzidi et al., 2002). Between these two sutures, the extent of the crustal thickening beneath the DSZ (averaging ~20 km, collision of two Archean microcontinents) is considerably larger than that beneath the STZ (by 5–10 km, collision of a Proterozoic Wabamun domain with an Archean Hearne craton), which may reflect differences both in the collisional/thickening processes over the last 1.8 Ga and in the rate of erosion. Judging from the history of the nearby THO, which has been recently likened to the evolution of the Tibetan plateau (Weller & St-Onge, 2017), both the surface elevation and the depth of the crustal root along the GFTZ during the Paleoproterozoic era most likely have been substantially greater than the present-day values (~50 km).

We find clear evidence of crustal thickening beneath the GFTZ via underplating, which is widely believed to be an efficient mechanism for crustal growth or differentiation under subduction or rifting environments (Furlong & Fountain, 1986; Rudnick & Gao, 2003; Thybo & Artemieva, 2013). A dense, high-velocity LCL could result from mantle magmatic intrusions and contain a mixture of mafic granulites, pyroxenites, and eclogite (Clowes et al., 2002; Thybo & Artemieva, 2013; Thurner et al., 2015). Partial eclogitization of the lower crust (Gilligan et al., 2016) under high-pressure, low-temperature metamorphism (e.g., in ocean-continent subduction zones; Darbyshire et al., 2017) may also play a role. Both northern Montana (Clowes et al., 2002; Gorman et al., 2002) and Colorado Plateau (Karlstrom et al., 2005), which are adjacent to the western Canadian platform, have been linked to rift-related underplating in the early Proterozoic (Barnhart et al., 2012; Mahan et al., 2012). A recent study by Schulte-Pelkum et al. (2017) systematically analyzes RFs from USArray data and provides compelling evidence of multiple RF conversions in the lower crust. Through waveform modeling they substantiate the existence of a high-velocity layer, which is corroborated by a recent crustal shear velocity model (Shen & Ritzwoller, 2016). This finding is supported by multiple lower crustal conversions in our stacked RFs and elevated Vp/Vs ratios for stations near the GFTZ, since the intrusion of mafic/ultramafic mantle melts would modify the lower crust and greatly increase the average Poisson's ratio within the crustal column (Christensen, 1996; Figure 12b). Similar observations of multiple crustal conversions and a deep Moho were documented along the THO directly east of our study region (Thurner et al., 2015; Weller & St-Onge, 2017). In other words, crustal underplating may be more pervasive during the Proterozoic eon than previously thought in western Laurentia.

5.5. Other Implications for the Tectonic Model and Constraints

Our model provides improved structural constraints for tectonic events surrounding the VS in southern Alberta. The VS is recognizable from an east-trending gravity and magnetic anomalies (Ross et al., 1991; Villeneuve et al., 1993) sandwiched between Archean-aged Hearne (north) and MHB (south; Eaton et al., 1999; Hoffman, 1988; Ross et al., 1991). While drill core samples suggest an early Proterozoic origin (Villeneuve et al., 1993), which post-dates the granitoids beneath the MHB (2.6–3.2 Ga; Ross et al., 1991; Villeneuve et al., 1993), interpretations of the 350-km-long VS vary broadly in age [i.e., Archean (Hoffman, 1988) versus Paleoproterozoic (i.e., Ross et al., 1991; Eaton et al., 1999)] and geometry [e.g., northward (Ross et al., 1991) versus southward (Eaton et al., 1999; Lemieux et al., 2000) dipping]. The nature of this semi-linear geological structure has also been debated among several competing hypotheses involving a failed continental rift (Kanasewich et al., 1969), an intraplate collision zone (Hoffman, 1990), and a Proterozoic suture separating (1) the Wyoming and Hearne cratons (Hoffman, 1988; Thomas et al., 1987) or (2) the MHB and Hearne craton (Eaton et al., 1999; Lemieux et al., 2000; Ross, 2000).

While the data coverage does not allow us to unequivocally resolve the crustal signatures surrounding VS, three nearby broadband seismic stations (see Figure 1) do provide a first-order assessment of this potential suture zone. Two of these stations suggest an anomalously deep Moho (see Figures 5a and 5b) and increased Vp/Vs ratios (see Figure 11a). These observations are, to first order, consistent with those of STZ and GFTZ. The relative positions of the Moho dip (south of the VS, which may be associated with the suture) and increased Vp/Vs ratio (north of the VS, the potential magmatic arc) appears to favor a north-dipping subduction morphology (Ross et al., 1991).

The common crustal seismic signatures from all three proposed boundary zones (STZ, VS, and GFTZ) in our study may have far-reaching implications for the overall tectonic history of western Laurentia. It was suggested earlier that, based on the proposed reset time of the GFTZ, the circum-Wyoming Proterozoic

tectonic events, for example, along THO and Great Falls, could all be at least partly coeval during the Proterozoic eon (Mueller et al., 2002). North of this region, overlapping ages of the basement rock samples from the WCSB have been strongly linked to a dual collisional (i.e., “Tectonic Vise”) model (Clowes et al., 2002; Ellis et al., 1998; Ross et al., 2000) centering around Hearne during the Paleoproterozoic era. Judging from similar rock ages ranging from 1.85 to 1.70 Ga from the basement of the WCSB and crustal characteristics (depressed Moho and high Vp/Vs ratios) near all three boundary zones, it is plausible that convergent tectonics dominated not only the Wyoming craton (Lemieux et al., 2000), but a broader Proterozoic lithosphere collisional system comprised of the Hearne, MHB, and Wyoming (one that we refer to as the “HMW system”; see Figure 12b). HMW experiences major compression and deformation due to plate convergences across the Tobacco Root Mountain in the west/southwest, THO in the east, and GFTZ/VS/STZ northeastward, resulting in thickening of continental crust (Chen et al., 2015) and the lithospheric mantle (e.g., Hearne Province; Bao & Eaton, 2015; Chen et al., 2017).

6. Conclusions

In this study, we analyze the broadband seismic data recorded by USArray and the most complete set of regional seismic networks to date. Our measurements show major improvements in the resolution of Moho depths and Vp/Vs ratios over existing regional and global models. Stacked RFs suggest lateral variations in Moho depth from the WCSB to the adjacent Cordillera, and strong gradients in Moho depth and Vp/Vs ratios across proposed Paleoproterozoic suture zones. Combining with existing potential field and geological observations, we are able to reach the following key conclusions.

1. We observe significant crustal thickening and Vp/Vs ratio increases near the STZ and GFTZ, which favor a collisional origin for both proposed tectonic boundaries.
2. We dispute the earlier geophysical definition of the GFTZ based on linear northeast striking potential field gradients near the U.S.-Canada border. The outcomes of our RF analysis suggest that the true suture is located ~150 km to the southeast within the TMO, consistent with earlier surface geological observations.
3. Based on confined zones of high Vp/Vs ratio and depressed Moho, we stipulate that the spatial extent of crustal underplating near the GFTZ is significantly smaller than earlier reported and is mainly confined to the TMO.

Finally, in view of similar rock ages from all parts of northern Montana and the WCSB basement, we conjecture that the Rae, Hearn, MHB, and Wyoming cratons were all active during the Paleoproterozoic era and their interactions, particularly coeval subductions and collisions, are largely responsible for the basement geology beneath western Laurentia.

Acknowledgments

We thank the host families of CRANE seismic stations for their long-term support of our work. Seismic data for USArray, CNSN, RAVEN, TD, PO, XN, and XR networks are provided by IRIS Data Management Center and Canadian National Data Centre. This work was supported by Natural Science and Engineering Research Council of Canada (NSERC; RGPIN-2017-06093). We thank two anonymous reviewers and the Associate Editor for constructive comments that improved the manuscript.

References

- Ammon, C. J. (1991). The isolation of receiver effects from teleseismic P waveforms. *Bulletin-Seismological Society of America*, 81(6), 2504–2510.
- Aulbach, S., Griffin, W. L., O'Reilly, S. Y., & McCandless, T. E. (2004). Genesis and evolution of the lithospheric mantle beneath the Buffalo Head Terrane, Alberta (Canada). *Lithos*, 77(1), 413–451.
- Bao, X., & Eaton, D. W. (2015). Large variations in lithospheric thickness of western Laurentia: Tectonic inheritance or collisional reworking? *Precambrian Research*, 266, 579–586.
- Bao, X., Eaton, D. W., & Gu, Y. J. (2016). Rayleigh wave azimuthally anisotropic phase velocity maps beneath western Canada. *Journal of Geophysical Research: Solid Earth*, 121, 1821–1834. <https://doi.org/10.1002/2015JB012453>
- Barnhart, K. R., Mahan, K. H., Blackburn, T. J., Bowring, S. A., & Dudas, F. O. (2012). Deep crustal xenoliths from central Montana, USA: Implications for the timing and mechanisms of high-velocity lower crust formation. *Geosphere*, 8(6), 1408–1428.
- Beaumont, C. (1981). Foreland basins. *Geophysical Journal of the Royal Astronomical Society*, 65(2), 291–329.
- Berman, R. G., Davis, W. J., & Pehrsson, S. (2007). Collisional Snowbird tectonic zone resurrected: Growth of Laurentia during the 1.9 Ga accretionary phase of the Hudsonian orogeny. *Geology*, 35(10), 911–914.
- Berman, R. G., Pehrsson, S., Davis, W. J., Ryan, J. J., Qui, H., & Ashton, K. E. (2013). The Arrowsmith orogeny: Geochronological and thermobarometric constraints on its extent and tectonic setting in the Rae craton, with implications for pre-Nuna supercontinent reconstruction. *Precambrian Research*, 232, 44–69.
- Boerner, D. E., Craven, J. A., Kurtz, R. D., Ross, G. M., & Jones, F. W. (1998). The Great Falls tectonic zone: Suture or intracontinental shear zone? *Canadian Journal of Earth Sciences*, 35(2), 175–183.
- Boerner, D. E., Kurtz, R. D., Craven, J. A., Rondenay, S., & Qian, W. (1995). Buried Proterozoic foredeep under the Western Canada sedimentary basin? *Geology*, 23(4), 297–300.
- Boerner, D. E., Kurtz, R. D., Craven, J. A., Ross, G. M., & Jones, F. W. (2000). A synthesis of electromagnetic studies in the Lithoprobe Alberta basement transect: constraints on Paleoproterozoic indentation tectonics. *Canadian Journal of Earth Sciences*, 37(11), 1509–1534.
- Bostock, M. G. (1996). Ps conversions from the upper mantle transition zone beneath the Canadian landmass. *Journal of Geophysical Research*, 101, 8393–8402.

- Bostock, M. G. (2013). The Moho in subduction zones. *Tectonophysics*, 609, 547–557.
- Bouzidi, Y., Schmitt, D. R., Burwash, R. A., & Kanasewich, E. R. (2002). Depth migration of deep seismic reflection profiles: Crustal thickness variations in Alberta. *Canadian Journal of Earth Sciences*, 39(3), 331–350.
- Buhlmann, A. L., Cavell, P., Burwash, R. A., Creaser, R. A., & Luth, R. W. (2000). Minette bodies and cognate mica-clinopyroxenite xenoliths from the Milk River area, southern Alberta: Records of a complex history of the northernmost part of the Archean Wyoming craton. *Canadian Journal of Earth Sciences*, 37(11), 1629–1650.
- Burwash, R. A., Chacko, T., Muehlenbachs, K., & Bouzidi, Y. (2000). Oxygen isotope systematics of the Precambrian basement of Alberta: Implications for Paleoproterozoic and Phanerozoic tectonics in northwestern Alberta. *Canadian Journal of Earth Sciences*, 37(11), 1611–1628.
- Calvert, A. J., Ramachandran, K., Kao, H., & Fisher, M. A. (2006). Local thickening of the Cascadia forearc crust and the origin of seismic reflectors in the uppermost mantle. *Tectonophysics*, 420(1), 175–188.
- Canil, D., Schulze, D. J., Hall, D., Hearn Jr, B. C., & Milliken, S. M. (2003). Lithospheric roots beneath western Laurentia: the geochemical signal in mantle garnets. *Canadian Journal of Earth Sciences*, 40(8), 1027–1051.
- Cassidy, J. F. (1992). Numerical experiments in broadband receiver function analysis. *Bulletin of the Seismological Society of America*, 82(3), 1453–1474.
- Cassidy, J. F. (1995). A comparison of the receiver structure beneath stations of the Canadian National Seismograph Network. *Canadian Journal of Earth Sciences*, 32(7), 938–951.
- Cavell, P. A., Burwash, R. A., & Nelson, D. B. (1993). Enriched mantle beneath southern Alberta: Isotopic evidence for a northern extension of the Wyoming block into southern Alberta. Geological Association of Canada–Mineralogical Association of Canada Program with Abstracts (Vol. 18, pp. A-17).
- Červený, V., & Soares, J. E. P. (1992). Fresnel volume ray tracing. *Geophysics*, 57(7), 902–915.
- Chacko, T., De, S. K., Creaser, R. A., & Muehlenbachs, K. (2000). Tectonic setting of the Talton magmatic zone at 1.9–2.0 Ga: A granitoid-based perspective. *Canadian Journal of Earth Sciences*, 37(11), 1597–1609.
- Chen, Y., Gu, Y. J., Dokht, R. M., & Sacchi, M. D. (2015). Crustal imprints of Precambrian orogenesis in western Laurentia. *Journal of Geophysical Research: Solid Earth*, 120, 6993–7012. <https://doi.org/10.1002/2014JB011353>
- Chen, Y., Gu, Y. J., & Hung, S. H. (2017). Finite-frequency P-wave tomography of the Western Canada sedimentary basin: Implications for the lithospheric evolution in western Laurentia. *Tectonophysics*, 698, 79–90.
- Chen, Y., Niu, F., Liu, R., Huang, Z., Tkalcic, H., Sun, L., & Chan, W. (2010). Crustal structure beneath China from receiver function analysis. *Journal of Geophysical Research*, 115, B03307. <https://doi.org/10.1029/2009JB006386>
- Christensen, N. I. (1996). Poisson's ratio and crustal seismology. *Journal of Geophysical Research*, 101, 3139–3156.
- Clowes, R. M., Burianyk, M. J., Gorman, A. R., & Kanasewich, E. R. (2002). Crustal velocity structure from SAREX, the southern Alberta refraction experiment. *Canadian Journal of Earth Sciences*, 39(3), 351–373.
- Clowes, R. M., White, D. J., & Hajnal, Z. (2010). Mantle heterogeneities and their significance: Results from Lithoprobe seismic reflection and refraction-wide-angle reflection studies This article is one of a series of papers published in this Special Issue on the theme Lithoprobe—parameters, processes, and the evolution of a continent. *Lithoprobe Contribution 1486. Canadian Journal of Earth Sciences*, 47(4), 409–443.
- Contenti, S. M., Gu, Y. J., & Shen, L. (2012). An integrated crustal analysis of craton-terrane transition. In AGU Fall Meeting Abstracts.
- Cousens, B. L., Aspler, L. B., Chiarenzelli, J. R., Donaldson, J. A., Sandeman, H., Peterson, T. D., & LeCheminant, A. N. (2001). Enriched Archean lithospheric mantle beneath western Churchill Province tapped during Paleoproterozoic orogenesis. *Geology*, 29(9), 827–830.
- Cox, K. G. (1993). Continental magmatic underplating. *Philosophical Transactions: Physical Sciences and Engineering*, 345, 155–166.
- Darbyshire, F. A., Bastow, I. D., Petrescu, L., Gilligan, A., & Thompson, D. A. (2017). A tale of two orogens: crustal processes in the Proterozoic Trans-Hudson and Grenville Orogens, eastern Canada. *Tectonics*, 36, 1633–1659. <https://doi.org/10.1002/2017TC004479>
- Dave, R., & Li, A. (2016). Destruction of the Wyoming craton: Seismic evidence and geodynamic processes. *Geology*, 44(11), 883–886.
- Davis, W. J., Berman, R., Kjarsgaard, B., & Ross, G. M. (1995). U–Pb geochronology and isotopic studies of crustal xenoliths from the Archean Medicine Hat block, northern Montana and southern Alberta: Paleoproterozoic reworking of Archean crust. In *Alberta Basement Transects Workshop: Lithoprobe Report* (Vol. 47, pp. 330–335).
- De Suman, K., Chacko, T., Creaser, R. A., & Muehlenbachs, K. (2000). Geochemical and Nd-Pb-O isotope systematics of granites from the Talton Magmatic Zone, NE Alberta: Implications for early Proterozoic tectonics in western Laurentia. *Precambrian Research*, 102(3), 221–249.
- Dueker, K. G., & Sheehan, A. F. (1997). Mantle discontinuity structure from midpoint stacks of converted P to S waves across the Yellowstone hotspot track. *Journal of Geophysical Research*, 102(B4), 8313–8327.
- Dziewonski, A. M., & Anderson, D. L. (1981). Preliminary reference Earth model. *Physics of the Earth and Planetary Interiors*, 25(4), 297–356.
- Eaton, D. W., & Cassidy, J. F. (1996). A relic Proterozoic subduction zone in western Canada: New evidence from seismic reflection and receiver function data. *Geophysical Research Letters*, 23, 3791–3794.
- Eaton, D. W., Ross, G. M., & Clowes, R. M. (1999). Seismic-reflection and potential-field studies of the Vulcan structure, western Canada: A Paleoproterozoic Pyrenees? *Journal of Geophysical Research*, 104, 23,255–23,269.
- Efron, B., & Tibshirani, R. (1986). Bootstrap methods for standard errors, confidence intervals, and other measures of statistical accuracy. *Statistical Science*, 1, 54–75.
- Ellis, S., Beaumont, C., Jamieson, R. A., & Quinlan, G. (1998). Continental collision including a weak zone: The vise model and its application to the Newfoundland Appalachians. *Canadian Journal of Earth Sciences*, 35(11), 1323–1346.
- Flowers, R. M., Bowring, S. A., Mahan, K. H., Williams, M. L., & Williams, I. S. (2008). Stabilization and reactivation of cratonic lithosphere from the lower crustal record in the western Canadian shield. *Contributions to Mineralogy and Petrology*, 156(4), 529.
- Flowers, R. M., Bowring, S. A., & Williams, M. L. (2006). Timescales and significance of high-pressure, high-temperature metamorphism and mafic dike anatexis, Snowbird tectonic zone, Canada. *Contributions to Mineralogy and Petrology*, 151(5), 558.
- Foster, D. A., Mueller, P. A., Mogk, D. W., Wooden, J. L., & Vogl, J. J. (2006). Proterozoic evolution of the western margin of the Wyoming craton: Implications for the tectonic and magmatic evolution of the northern Rocky Mountains. *Canadian Journal of Earth Sciences*, 43(10), 1601–1619.
- Frassetto, A., & Thybo, H. (2013). Receiver function analysis of the crust and upper mantle in Fennoscandia—isostatic implications. *Earth and Planetary Science Letters*, 381, 234–246.
- Furlong, K. P., & Fountain, D. M. (1986). Continental crustal underplating: Thermal considerations and seismic-petrologic consequences. *Journal of Geophysical Research*, 91, 8285–8294.
- Fyfe, W. S. (1992). Magma underplating of continental crust. *Journal of Volcanology and Geothermal Research*, 50(1–2), 33–40.
- Gibb, R. A., & Walcott, R. I. (1971). A Precambrian suture in the Canadian shield. *Earth and Planetary Science Letters*, 10(4), 417–422.

- Gilbert, H. (2012). Crustal structure and signatures of recent tectonism as influenced by ancient terranes in the western United States. *Geosphere*, 8(1), 141–157.
- Giletti, B. J. (1966). Isotopic ages from southwestern Montana. *Journal of Geophysical Research*, 71, 4029–4036.
- Gilligan, A., Bastow, I. D., & Darbyshire, F. A. (2016). Seismological structure of the 1.8 Ga Trans-Hudson orogen of North America. *Geochemistry, Geophysics, Geosystems*, 17, 2421–2433. <https://doi.org/10.1002/2016GC006419>
- Godin, L., Grujic, D., Law, R. D., & Searle, M. P. (2006). Channel flow, ductile extrusion and exhumation in continental collision zones: An introduction. *Tectonophysics*, 430(1–4), 1–16.
- Gorman, A. R., Clowes, R. M., Ellis, R. M., Henstock, T. J., Spence, G. D., Keller, G. R., et al. (2002). Deep probe: Imaging the roots of western North America. *Canadian Journal of Earth Sciences*, 39(3), 375–398.
- Gu, Y. J., Chen, Y., & Hung, S. H. (2016). P and S wave finite-frequency imaging of the Cordillera-craton boundary zone in Western Canada. In AGU Fall Meeting Abstracts.
- Gu, Y. J., Okeler, A., Shen, L., & Contenti, S. (2011). The Canadian Rockies and Alberta Network (CRANE): New constraints on the Rockies and western Canada sedimentary basin. *Seismological Research Letters*, 82(4), 575–588.
- Gu, Y. J., & Shen, L. (2015). Noise correlation tomography of Southwest Western Canada sedimentary basin. *Geophysical Journal International*, 202(1), 142–162.
- Gu, Y. J., Zhang, Y., Sacchi, M. D., Chen, Y., & Contenti, S. (2015). Sharp mantle transition from cratons to Cordillera in southwestern Canada. *Journal of Geophysical Research: Solid Earth*, 120, 5051–5069. <https://doi.org/10.1002/2014JB011802>
- Hanmer, S., Parrish, R., Williams, M., & Kopf, C. (1994). Striding-Athabasca mylonite zone: Complex Archean deep-crustal deformation in the East Athabasca mylonite triangle, northern Saskatchewan. *Canadian Journal of Earth Sciences*, 31(8), 1287–1300.
- Hanmer, S., & Relf, C. (2000). Western Churchill NATMAP Project: New results and potential significance. *Proceedings of GeoCanada*, 4.
- Hanmer, S., Williams, M., & Kopf, C. (1995). Striding-Athabasca mylonite zone: Implications for the Archean and Early Proterozoic tectonics of the western Canadian shield. *Canadian Journal of Earth Sciences*, 32(2), 178–196.
- Haschke, M., & Günther, A. (2003). Balancing crustal thickening in arcs by tectonic vs. magmatic means. *Geology*, 31(11), 933–936.
- Hayden, R. J., & Wehrenberg, J. P. (1960). Dating of igneous and metamorphic rocks in Western Montana. *The Journal of Geology*, 68(1), 94–97.
- Heaman, L. M. (1994). 2.45 Ga global mafic magmatism: Earth's oldest superplume. In M. A. Lanphere, G. B. Dalrymple, & B. D. Turrin (Eds.), *8th International Conference on Geochronology, Cosmochemistry and Isotope Geology* (Vol. 1107, 132 pp.). United States Geological Survey, Circular.
- Heaman, L. M., & LeCheminant, A. N. (1993). Paragenesis and U-Pb systematics of baddeleyite (ZrO₂). *Chemical Geology*, 110(1–3), 95–126.
- Henstock, T. J., Levander, A., Snelson, C. M., Keller, G. R., Miller, K. C., Harder, S. H., et al. (1998). Probing the Archean and Proterozoic lithosphere of western North America. *GSA Today*, 8(7), 1–5.
- Hoffman, P. F. (1988). United Plates of America, the birth of a craton: Early Proterozoic assembly and growth of Laurentia. *Annual Review of Earth and Planetary Sciences*, 16(1), 543–603.
- Hoffman, P. F. (1989). Speculations on Laurentia's first gigayear (2.0 to 1.0 Ga). *Geology*, 17(2), 135–138.
- Hoffman, P. F. (1990). Subdivision of the Churchill Province and the extent of the Trans-Hudson orogen. In *The Early Proterozoic Trans-Hudson Orogen of North America* (pp. 15–39). St. John's, Canada: Geological Association of Canada.
- Holm, D., & Schneider, D. (2002). ⁴⁰Ar/³⁹Ar evidence for ca. 1800 Ma tectonothermal activity along the Great Falls tectonic zone, central Montana. *Canadian Journal of Earth Sciences*, 39(12), 1719–1728.
- Hope, J., & Eaton, D. (2002). Crustal structure beneath the Western Canada sedimentary basin: Constraints from gravity and magnetic modelling. *Canadian Journal of Earth Sciences*, 39(3), 291–312.
- Hung, S. H., Shen, Y., & Chiao, L. Y. (2004). Imaging seismic velocity structure beneath the Iceland hot spot: A finite frequency approach. *Journal of Geophysical Research*, 109(B8), B08305. <https://doi.org/10.1029/2003JB002889>
- Julià, J., Herrmann, R. B., Ammon, C. J., & Akinci, A. (2004). Evaluation of deep sediment velocity structure in the New Madrid Seismic Zone. *Bulletin of the Seismological Society of America*, 94(1), 334–340.
- Kanasewich, E. R., Clowes, R. M., & McCloskey, C. H. (1969). A buried Precambrian rift in western Canada. *Tectonophysics*, 8(4–6), 513–527.
- Kao, H., Behr, Y., Currie, C. A., Hyndman, R., Townend, J., Lin, F. C., et al. (2013). Ambient seismic noise tomography of Canada and adjacent regions: Part I. Crustal structures. *Journal of Geophysical Research: Solid Earth*, 118, 5865–5887. <https://doi.org/10.1029/2013JB010535>
- Karlstrom, K. E., Whitmeyer, S. J., Dueker, K., Williams, M. L., Bowring, S. A., Levander, A. R., et al. (2005). Synthesis of results from the Cd-Rom experiment: 4-D image of the lithosphere beneath the Rocky Mountains and implications for understanding the evolution of continental lithosphere. In *Rocky Mountain Region: An Evolving Lithosphere Tectonics, Geochemistry, and Geophysics, Geophysical Monograph Series* (Vol. 154, pp. 421–441). New Jersey: Wiley.
- Karlstrom, L., Lee, C. T., & Manga, M. (2014). The role of magmatically driven lithospheric thickening on arc front migration. *Geochemistry, Geophysics, Geosystems*, 15, 2655–2675. <https://doi.org/10.1029/2014GC005355>
- Kennett, B. L. N., Engdahl, E. R., & Buland, R. (1995). Constraints on seismic velocities in the Earth from traveltimes. *Geophysical Journal International*, 122(1), 108–124.
- Langston, C. A. (1977). Corvallis, Oregon, crustal and upper mantle receiver structure from teleseismic P and S waves. *Bulletin of the Seismological Society of America*, 67(3), 713–724.
- Laske, G., Masters, G., Ma, Z., & Pasyanos, M. (2013). Update on CRUST1. 0—A 1-degree global model of Earth's crust. In *Geophys. Res. Abstracts* (Vol. 15, p. 20132658abstrEGU),
- Lemieux, S., Ross, G. M., & Cook, F. A. (2000). Crustal geometry and tectonic evolution of the Archean crystalline basement beneath the southern Alberta Plains, from new seismic reflection and potential-field studies. *Canadian Journal of Earth Sciences*, 37(11), 1473–1491.
- Levander, A., & Miller, M. S. (2012). Evolutionary aspects of lithosphere discontinuity structure in the western US. *Geochemistry, Geophysics, Geosystems*, 13, Q0AK07. <https://doi.org/10.1029/2012GC004056>
- Levin, V., & Park, J. (1997). Crustal anisotropy in the Ural Mountains foredeep from teleseismic receiver functions. *Geophysical Research Letters*, 24, 1283–1286.
- Ligorría, J. P., & Ammon, C. J. (1999). Iterative deconvolution and receiver-function estimation. *Bulletin of the Seismological Society of America*, 89(5), 1395–1400.
- Lowry, A. R., & Pérez-Gussinyé, M. (2011). The role of crustal quartz in controlling Cordilleran deformation. *Nature*, 471(7338), 353.
- MacRae, N. D., Armitage, A. E., Miller, A. R., Roddick, J. C., Jones, A. L., & Mudry, M. P. (1996). The diamondiferous Aklulik lamprophyre dyke, Gibson Lake area, NWT. In *Searching for diamonds in Canada*, Geological Survey of Canada, Open File 3228 (268 pp.). Ottawa. <https://doi.org/10.4095/208202>

- Mahan, K. H., Schulte-Pelkum, V., Blackburn, T. J., Bowring, S. A., & Dudas, F. O. (2012). Seismic structure and lithospheric rheology from deep crustal xenoliths, central Montana, USA. *Geochemistry, Geophysics, Geosystems*, 13, Q10012. <https://doi.org/10.1029/2012GC004332>
- Mahan, K. H., & Williams, M. L. (2005). Reconstruction of a large deep-crustal terrane: Implications for the Snowbird tectonic zone and early growth of Laurentia. *Geology*, 33(5), 385–388.
- Mueller, P. A., & Frost, C. D. (2006). The Wyoming Province: A distinctive Archean craton in Laurentian North America. *Canadian Journal of Earth Sciences*, 43(10), 1391–1397.
- Mueller, P. A., Heatherington, A. L., Kelly, D. M., Wooden, J. L., & Mogk, D. W. (2002). Paleoproterozoic crust within the Great Falls tectonic zone: Implications for the assembly of southern Laurentia. *Geology*, 30(2), 127–130.
- Mueller, P. A., Shuster, R. D., D'Arcy, K. A., Heatherington, A. L., Nutman, A. P., & Williams, I. S. (1995). Source of the northeastern Idaho Batholith: Isotopic evidence for a Paleoproterozoic terrane in the northwestern US. *The Journal of Geology*, 103(1), 63–72.
- Nieuwenhuis, G., Unsworth, M. J., Pana, D., Craven, J., & Bertrand, E. (2014). Three-dimensional resistivity structure of Southern Alberta, Canada: Implications for Precambrian tectonics. *Geophysical Journal International*, 197(2), 838–859.
- Niu, F., Bravo, T., Pavlis, G., Vernon, F., Rendon, H., Bezada, M., & Levander, A. (2007). Receiver function study of the crustal structure of the southeastern Caribbean plate boundary and Venezuela. *Journal of Geophysical Research*, 112, B11308. <https://doi.org/10.1029/2006JB004802>
- O'Neill, J. M. (1998). The Great Falls tectonic zone, Montana–Idaho: An early Proterozoic collisional orogen beneath and south of the Belt Basin. In Belt Symposium III—1993: Montana Bureau of Mines and Geology Special Publication (Vol. 112, pp. 222–228).
- O'Neill, J. M. (2007). Great Divide megashear, Montana and Idaho: An intraplate lithospheric shear zone and its impact on Mesoproterozoic depositional basins. In *Geol. Soc. Am. Abstr. Programs* (Vol. 39, p. 36).
- O'Neill, J. M., & Lopez, D. A. (1985). Character and regional significance of Great Falls tectonic zone, east-central Idaho and west-central Montana. *AAPG Bulletin*, 69(3), 437–447.
- Pana, D. I. (2003). *Precambrian Basement of the Western Canada Sedimentary Basin in Northern Alberta*. Alberta Geological Survey.
- Pasyanos, M. E., Masters, T. G., Laske, G., & Ma, Z. (2014). LITHO1.0: An updated crust and lithospheric model of the Earth. *Journal of Geophysical Research: Solid Earth*, 119, 2153–2173. <https://doi.org/10.1002/2013JB010626>
- Paul, A., Kaviani, A., Hatzfeld, D., Vergne, J., & Mokhtari, M. (2006). Seismological evidence for crustal-scale thrusting in the Zagros mountain belt (Iran). *Geophysical Journal International*, 166(1), 227–237.
- Pirouz, M., Avouac, J. P., Hassanzadeh, J., Kirschvink, J. L., & Bahroudi, A. (2017). Early Neogene foreland of the Zagros, implications for the initial closure of the Neo-Tethys and kinematics of crustal shortening. *Earth and Planetary Science Letters*, 477, 168–182.
- Porritt, R. W., Allen, R. M., & Pollitz, F. F. (2014). Seismic imaging east of the Rocky Mountains with USArray. *Earth and Planetary Science Letters*, 402, 16–25.
- Regan, S. P., Williams, M. L., Chiarenzelli, J. R., Grohn, L., Mahan, K. H., & Gallagher, M. (2017). Isotopic evidence for Neoarchean continuity across the Snowbird tectonic zone, western Churchill Province, Canada. *Precambrian Research*, 300, 201–222.
- Rondenay, S. (2009). Upper mantle imaging with array recordings of converted and scattered teleseismic waves. *Surveys in Geophysics*, 30(4–5), 377–405.
- Ross, G. M. (2000). Introduction to special issue of Canadian Journal of Earth Sciences: The Alberta basement transect of Lithoprobe. *Canadian Journal of Earth Sciences*, 37(11), 1447–1452.
- Ross, G. M. (2002). Evolution of Precambrian continental lithosphere in Western Canada: Results from Lithoprobe studies in Alberta and beyond. *Canadian Journal of Earth Sciences*, 39(3), 413–437.
- Ross, G. M., & Eaton, D. W. (1997). Winagami reflection sequence: Seismic evidence for postcollisional magmatism in the Proterozoic of western Canada. *Geology*, 25(3), 199–202.
- Ross, G. M., & Eaton, D. W. (2002). Proterozoic tectonic accretion and growth of western Laurentia: Results from Lithoprobe studies in northern Alberta. *Canadian Journal of Earth Sciences*, 39(3), 313–329.
- Ross, G. M., Eaton, D. W., Boerner, D. E., & Miles, W. (2000). Tectonic entrapment and its role in the evolution of continental lithosphere: An example from the Precambrian of western Canada. *Tectonics*, 19, 116–134.
- Ross, G. M., McNicoll, V. J., Geldsetzer, H. H. J., Parrish, R. R., Carr, S. D., & Kinsman, A. (1993). Detrital zircon geochronology of Siluro-Devonian sandstones, Rocky Mountains, northeastern British Columbia. *Bulletin of Canadian Petroleum Geology*, 41(3), 349–357.
- Ross, G. M., Milkereit, B., Eaton, D., White, D., Kanasewich, E. R., & Burianyk, M. J. (1995). Paleoproterozoic collisional orogen beneath the western Canada sedimentary basin imaged by Lithoprobe crustal seismic-reflection data. *Geology*, 23(3), 195–199.
- Ross, G. M., Parrish, R. R., Villeneuve, M. E., & Bowring, S. A. (1991). Geophysics and geochronology of the crystalline basement of the Alberta Basin, western Canada. *Canadian Journal of Earth Sciences*, 28(4), 512–522.
- Rudnick, R. L., & Gao, S. (2003). Composition of the continental crust. *Treatise on Geochemistry*, 3, 659.
- Ryberg, T., & Weber, M. (2000). Receiver function arrays: A reflection seismic approach. *Geophysical Journal International*, 141(1), 1–11.
- Schmandt, B., & Lin, F. C. (2014). P and S wave tomography of the mantle beneath the United States. *Geophysical Research Letters*, 41(18), 6342–6349. <https://doi.org/10.1002/2014GL061231>
- Schulte-Pelkum, V., Mahan, K., Shen, W., & Stachnik, J. (2017). The distribution and composition of high-velocity lower crust across the continental US: Comparison of seismic and xenolith data and implications for lithospheric dynamics and history. *Tectonics*, 36, 1455–1496. <https://doi.org/10.1029/2017TC004480>
- Schultz, R., & Stern, V. (2015). The Regional Alberta Observatory for Earthquake Studies Network (RAVEN). *CSEG Recorder*, 40(8), 34–37.
- Schutt, D. L., Dueker, K., & Yuan, H. (2008). Crust and upper mantle velocity structure of the Yellowstone hot spot and surroundings. *Journal of Geophysical Research*, 113, B03310. <https://doi.org/10.1029/2007JB005109>
- Sheehan, A. F., Abers, G. A., Jones, C. H., & Lerner-Lam, A. L. (1995). Crustal thickness variations across the Colorado Rocky Mountains from teleseismic receiver functions. *Journal of Geophysical Research*, 100, 20,391–20,404.
- Shen, W., & Ritzwoller, M. H. (2016). Crustal and uppermost mantle structure beneath the United States. *Journal of Geophysical Research: Solid Earth*, 121, 4306–4342. <https://doi.org/10.1002/2016JB012887>
- Shen, W., Ritzwoller, M. H., & Schulte-Pelkum, V. (2013). A 3-D model of the crust and uppermost mantle beneath the central and western US by joint inversion of receiver functions and surface wave dispersion. *Journal of Geophysical Research: Solid Earth*, 118, 262–276. <https://doi.org/10.1029/2012JB009602>
- Shragge, J., Bostock, M. G., Bank, C. G., & Ellis, R. M. (2002). Integrated teleseismic studies of the southern Alberta upper mantle. *Canadian Journal of Earth Sciences*, 39(3), 399–411.
- Sims, P. K., Lund, K., & Anderson, E. (2005). Precambrian crystalline basement map of Idaho—An interpretation of aeromagnetic anomalies (No. 2884).
- Sims, P. K., O'Neill, J. M., Bankey, V., & Anderson, E. (2004). Precambrian basement geologic map of Montana—An interpretation of aeromagnetic anomalies (No. 2829).

- Snelson, C. M., Henstock, T. J., Keller, G. R., Miller, K. C., & Levander, A. (1998). Crustal and uppermost mantle structure along the Deep Probe seismic profile. *Rocky Mountain Geology*, 33(2), 181–198.
- Stern, R. J. (2002). Subduction zones. *Reviews of Geophysics*, 40(4), 10–12. <https://doi.org/10.1029/2001RG000108>
- Tesauro, M., Kaban, M. K., Mooney, W. D., & Cloetingh, S. (2014). NACr14: A 3D model for the crustal structure of the North American Continent. *Tectonophysics*, 631, 65–86.
- Thomas, M. D., Sharpton, V. L., & Grieve, R. A. F. (1987). Gravity patterns and Precambrian structure in the North American central plains. *Geology*, 15(6), 489–492.
- Thurner, S., Margolis, R., Levander, A., & Niu, F. (2015). PdS receiver function evidence for crustal scale thrusting, relic subduction, and mafic underplating in the Trans-Hudson Orogen and Yavapai province. *Earth and Planetary Science Letters*, 426, 13–22.
- Thybo, H., & Artemieva, I. M. (2013). Moho and magmatic underplating in continental lithosphere. *Tectonophysics*, 609, 605–619.
- Villeneuve, M. E., Ross, G. M., Theriault, R. J., & Miles, W. (1993). Tectonic subdivision and U-Pb geochronology of the crystalline basement of the Alberta Basin, western Canada.
- Vinnik, L. P. (1977). Detection of waves converted from P to SV in the mantle. *Physics of the Earth and Planetary Interiors*, 15(1), 39–45.
- Welford, J. K., & Clowes, R. M. (2006). Three-dimensional seismic reflection investigation of the upper crustal Winagami sill complex of northwestern Alberta, Canada. *Geophysical Journal International*, 166(1), 155–169.
- Weller, O. M., & St-Onge, M. R. (2017). Record of modern-style plate tectonics in the Palaeoproterozoic Trans-Hudson orogen. *Nature Geoscience*, 10(4), 305–311.
- Whitmeyer, S. J., & Karlstrom, K. E. (2007). Tectonic model for the Proterozoic growth of North America. *Geosphere*, 3(4), 220–259.
- Yeck, W. L., Sheehan, A. F., & Schulte-Pelkum, V. (2013). Sequential H-k stacking to obtain accurate crustal thicknesses beneath sedimentary basins. *Bulletin of the Seismological Society of America*, 103(3), 2142–2150.
- Yousof, M., Thybo, H., Artemieva, I. M., & Levander, A. (2015). Upper mantle structure beneath southern African cratons from seismic finite-frequency P-and S-body wave tomography. *Earth and Planetary Science Letters*, 420, 174–186.
- Yuan, X., Sobolev, S. V., Kind, R., Oncken, O., Bock, G., Asch, G., et al. (2000). Subduction and collision processes in the Central Andes constrained by converted seismic phases. *Nature*, 408(6815), 958.
- Zandt, G., & Ammon, C. J. (1995). Continental crust composition constrained by measurements of crustal Poisson's ratio. *Nature*, 374(6518), 152–154.
- Zhu, L., & Kanamori, H. (2000). Moho depth variation in southern California from teleseismic receiver functions. *Journal of Geophysical Research*, 105, 2969–2980.